GRAN SASSO
SCIENCE INSTITUTE

Low-frequency sensitivity limitations in current and future gravitational-wave detectors

Tomislav Andrić
Jan Harms

Program

0 Introduction

1 Sardinia site

2 Finite-element simulations

3 Results

4 Significance

5 Alignment sensing and control

Introduction

- Einstein Telescope
- Inspiral phase of compact binaries (NS, SMBH)

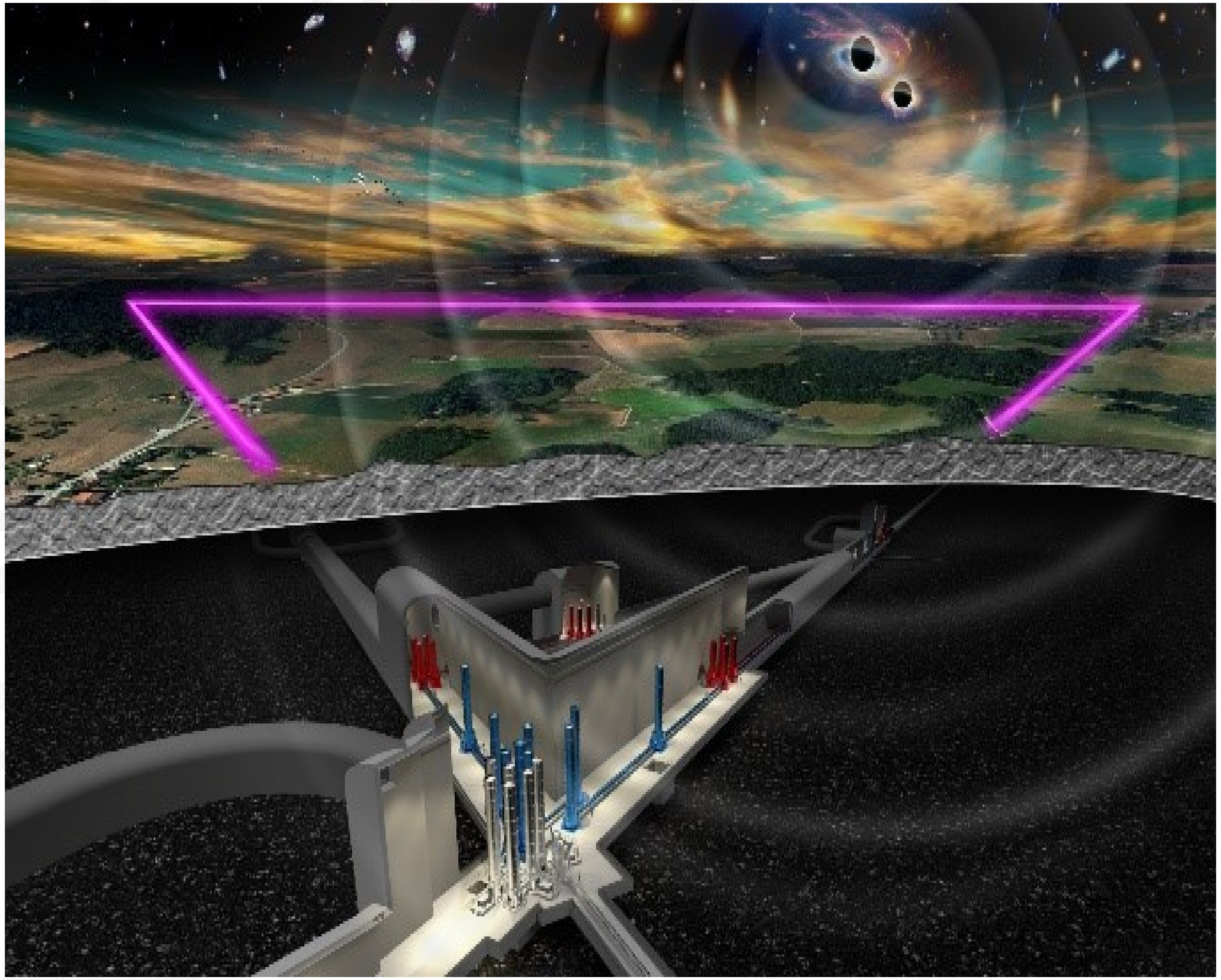

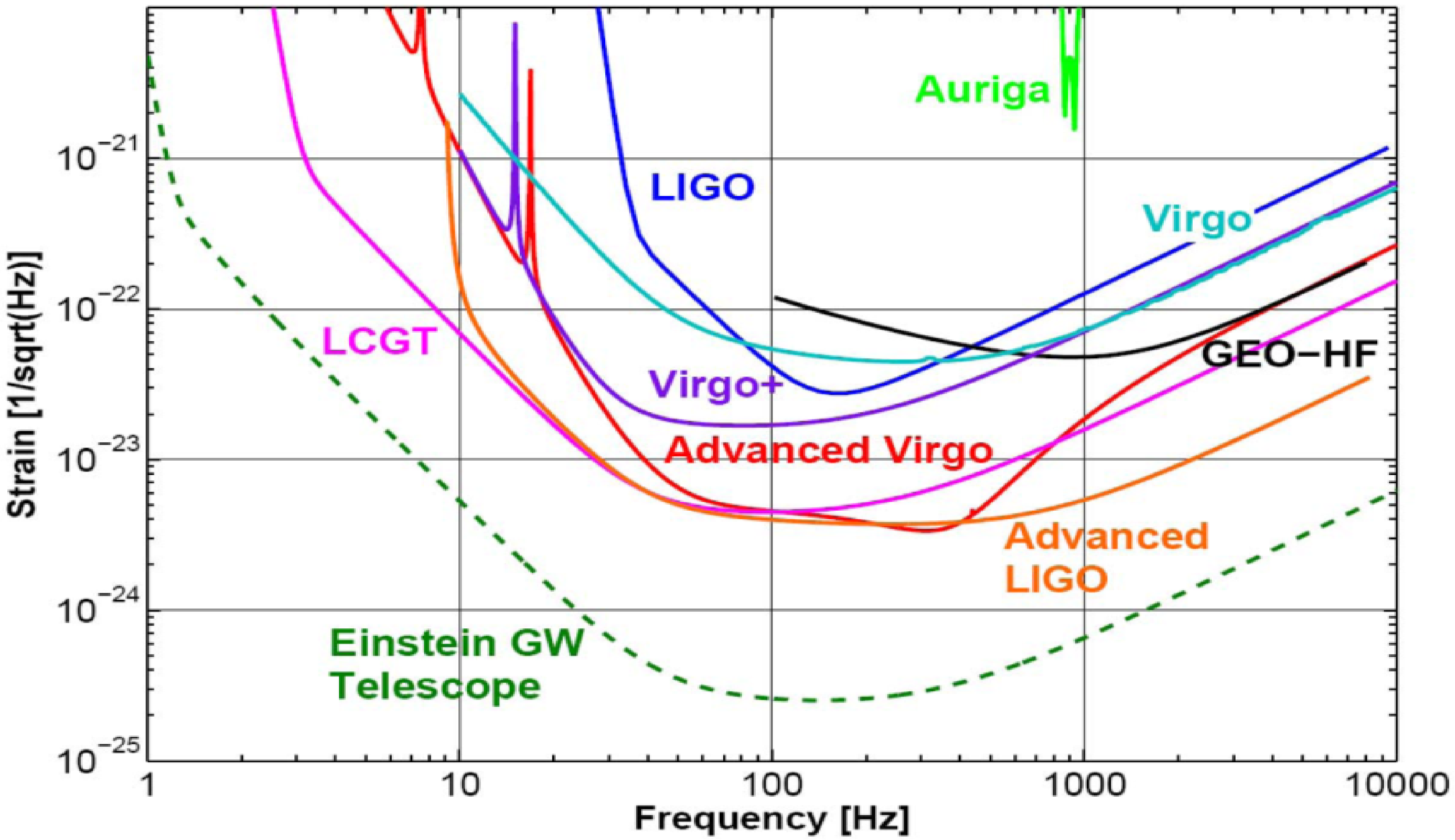

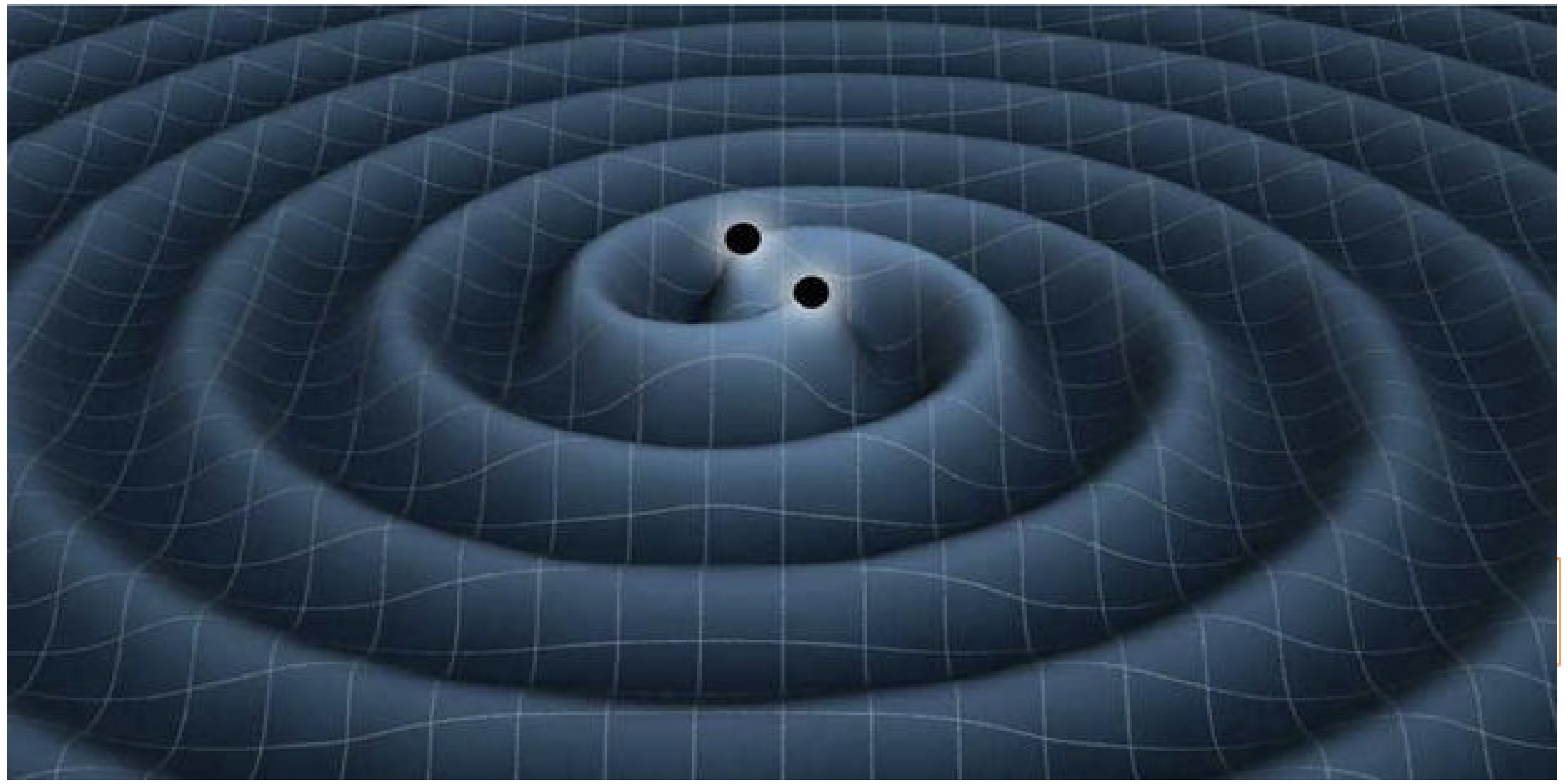

Introduction

- Seismic gravity gradient noise:
  1. Seismic surface displacement
  2. (De)compression of rock
  3. Displacement of underground cavern walls

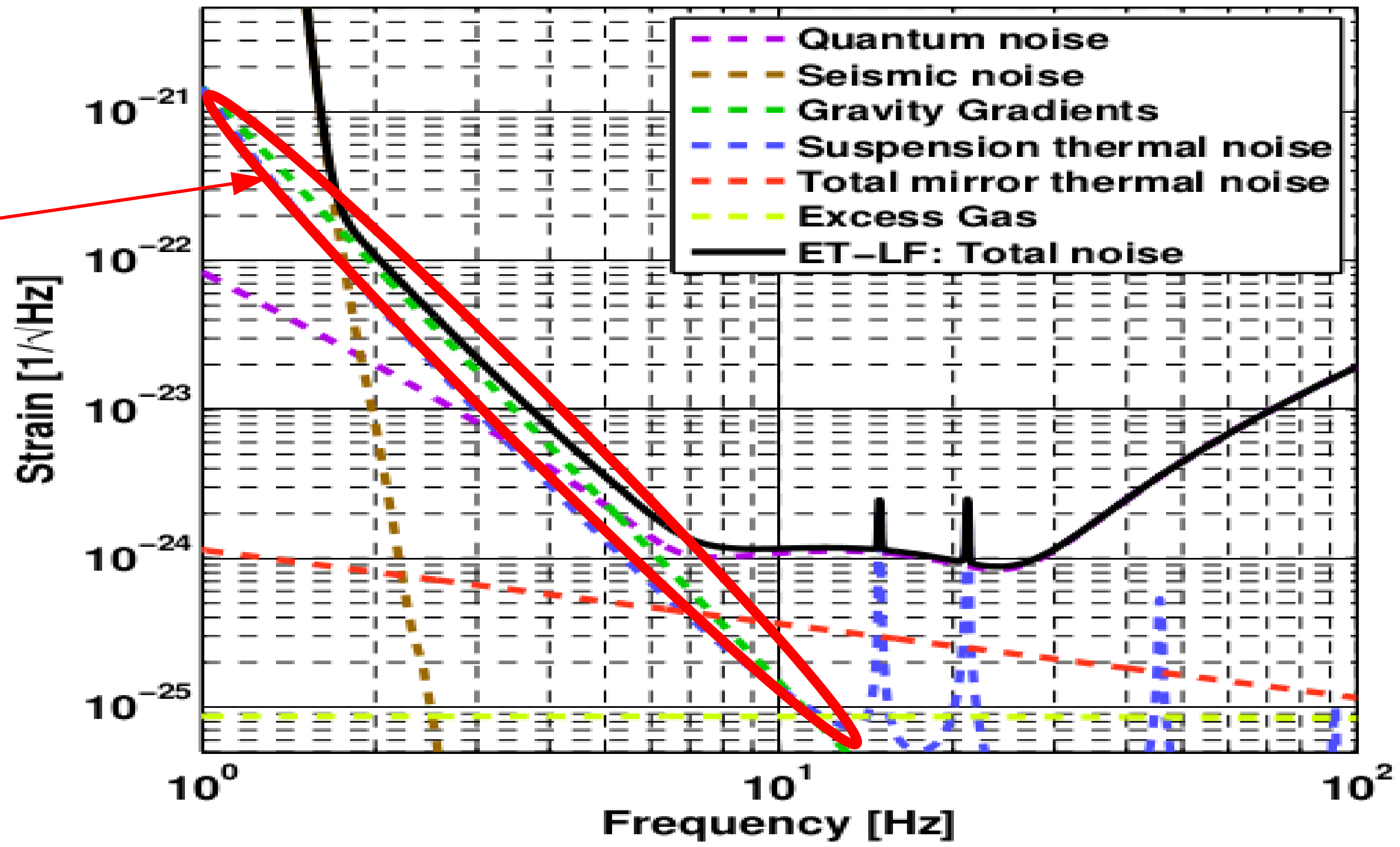

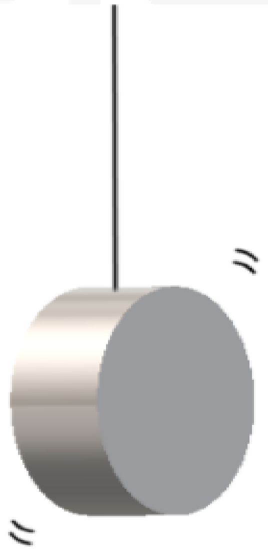

$$\delta\rho \rightarrow NN$$

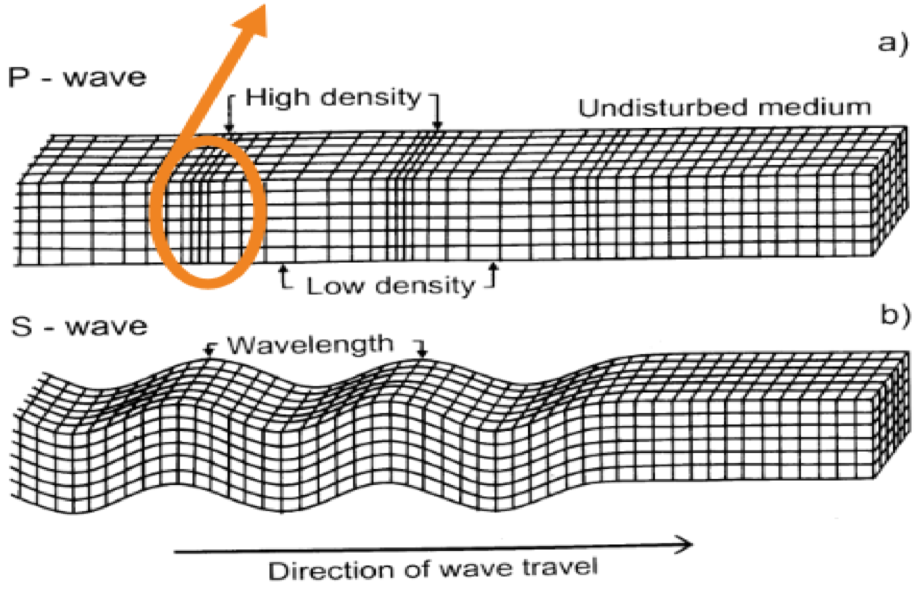

- Surface and underground locations of ET

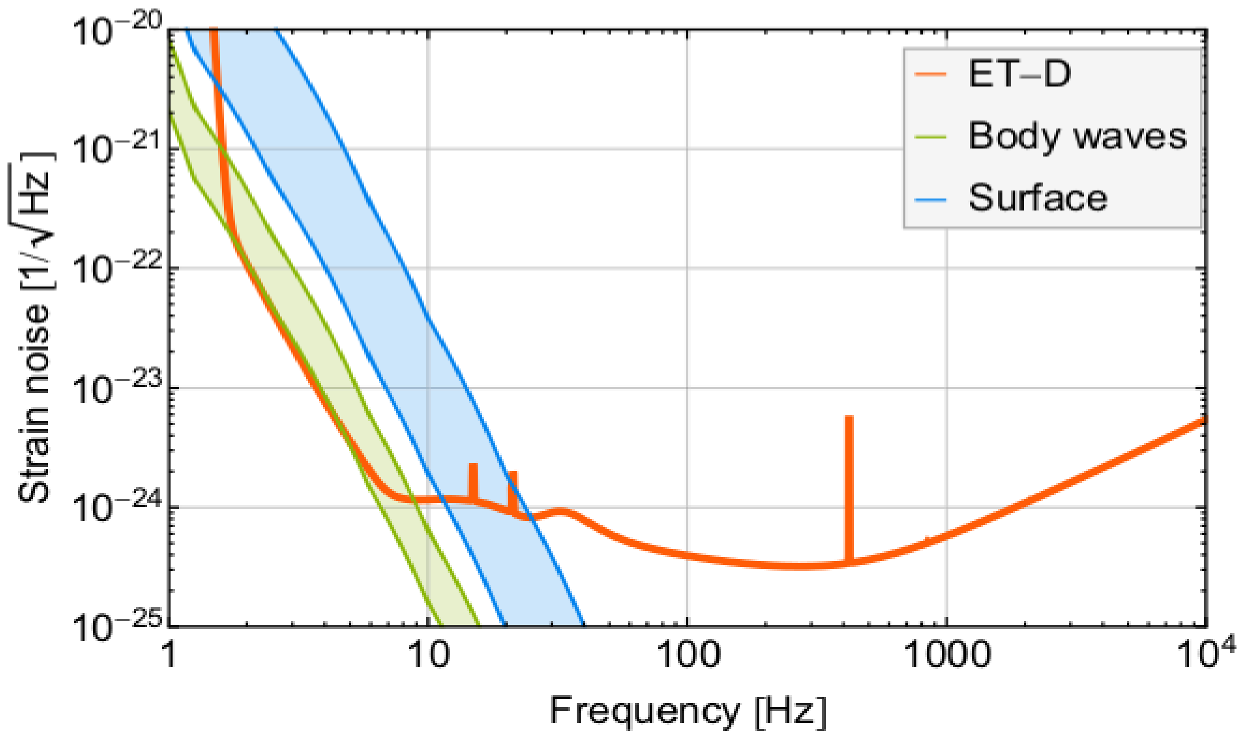

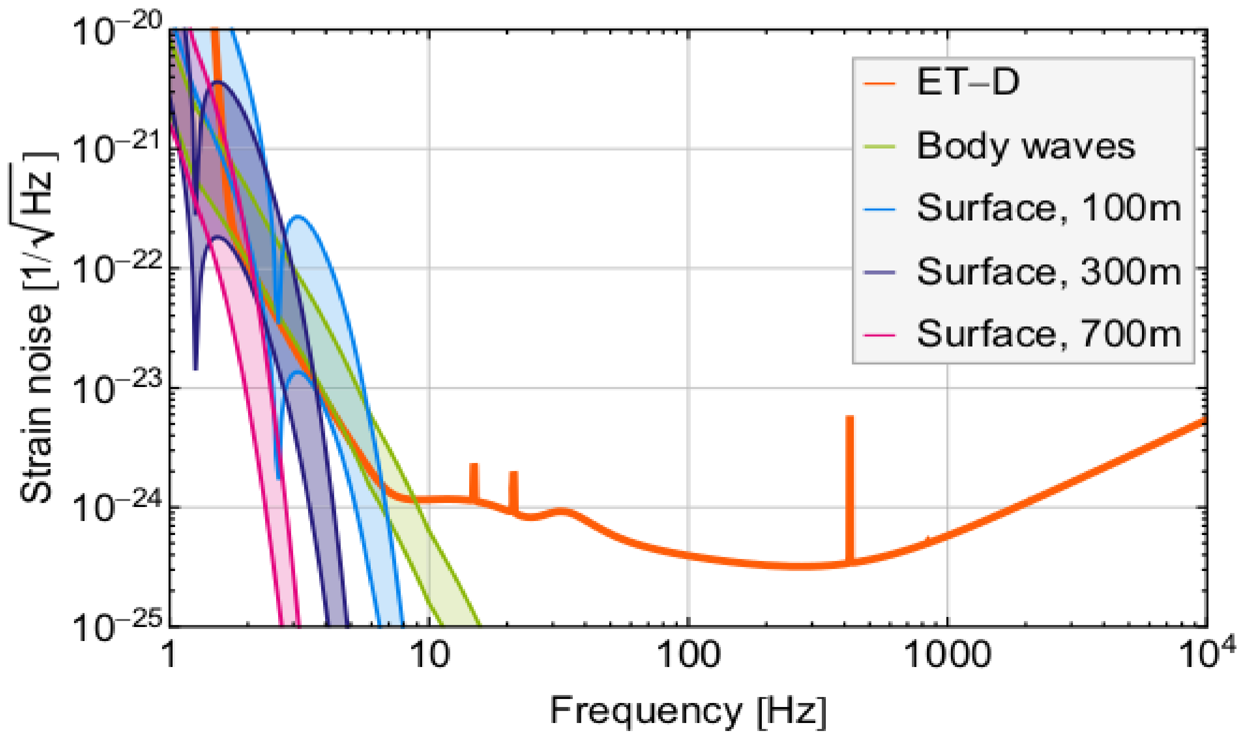

Sardinia site

- Topographic scattering
- Vertex A3

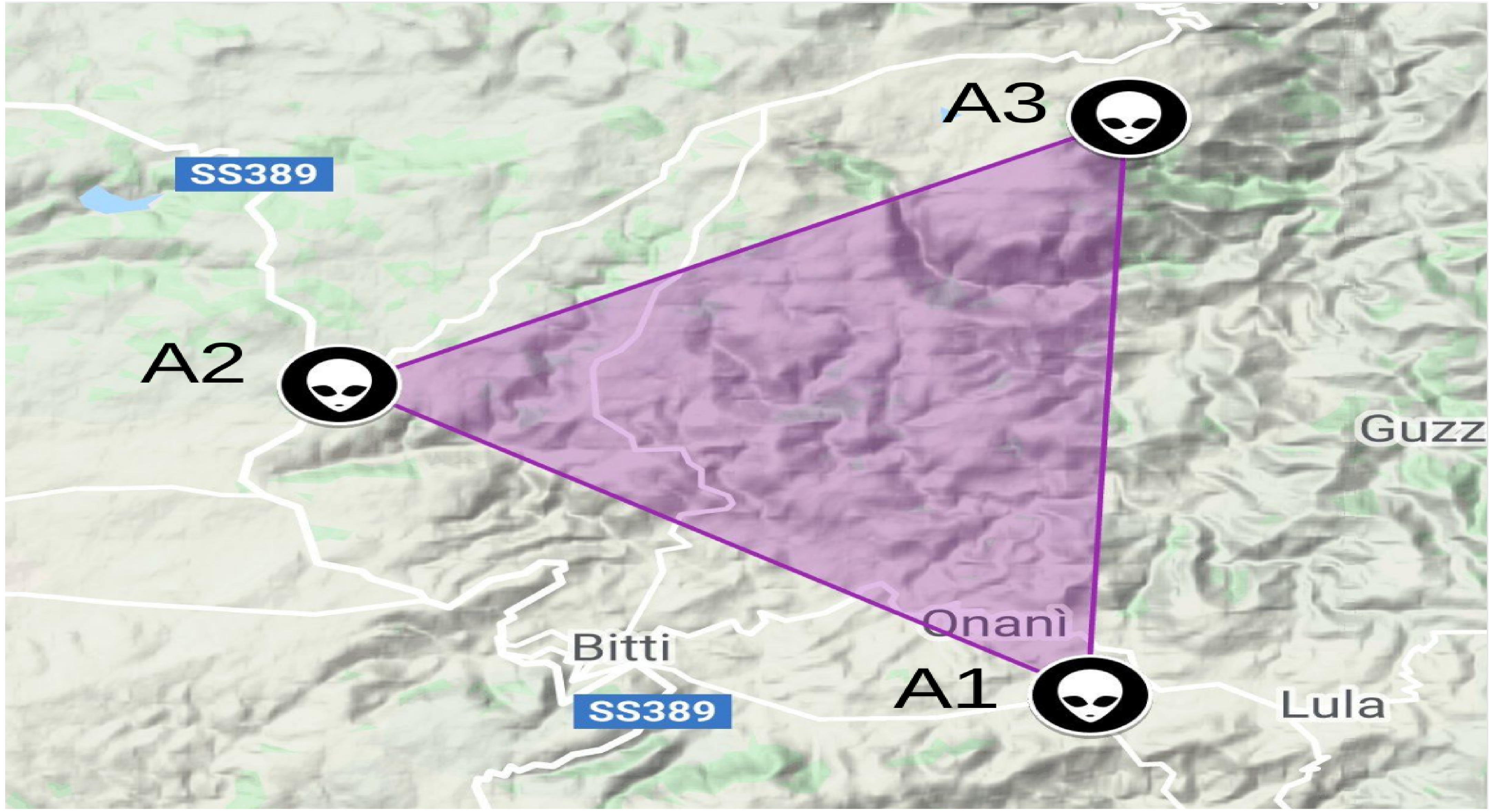

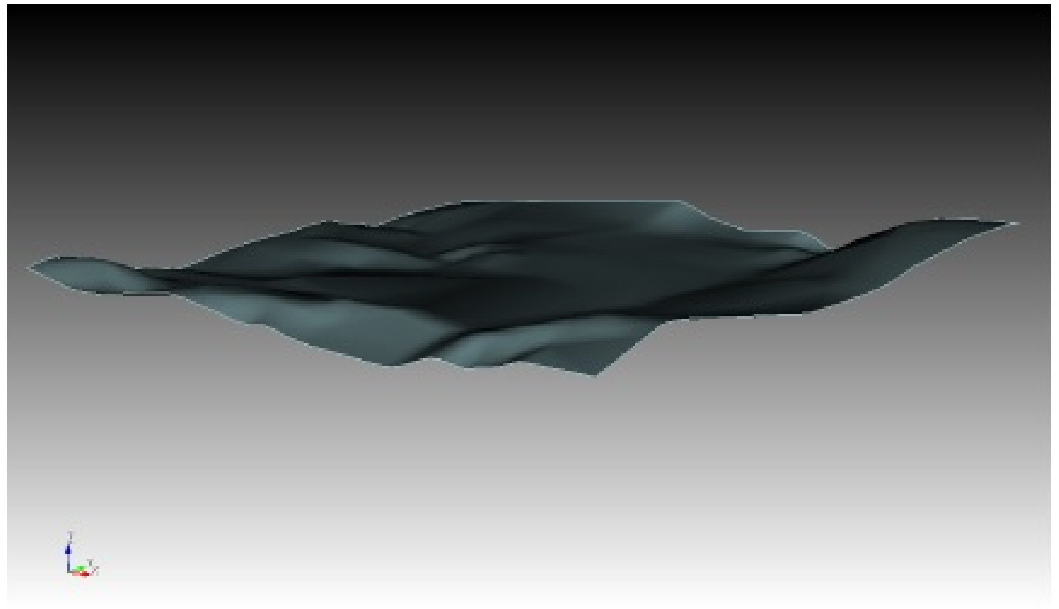
(a) Vertex A1

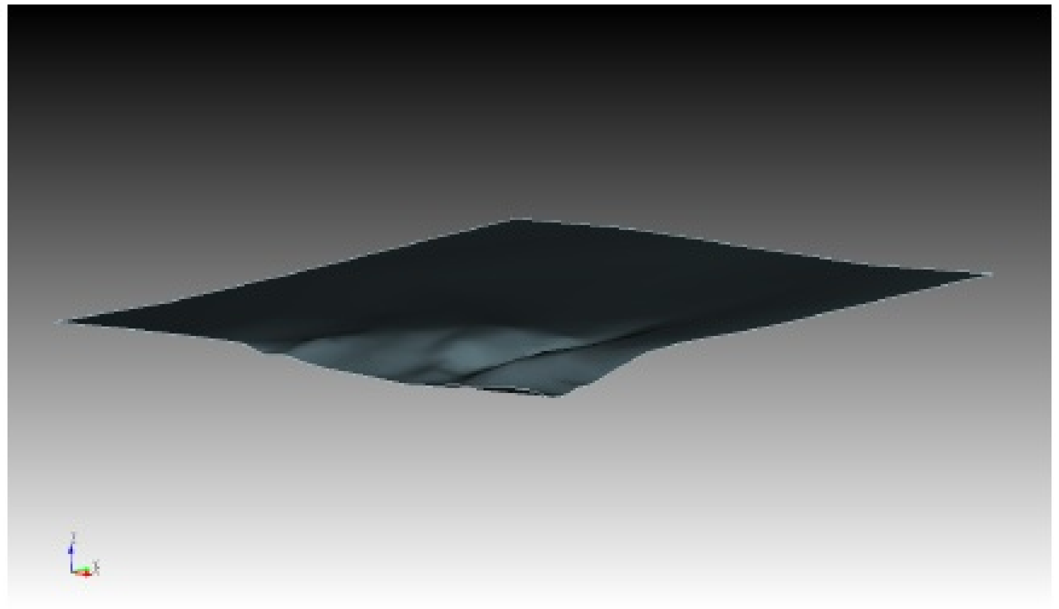
(b) Vertex A2

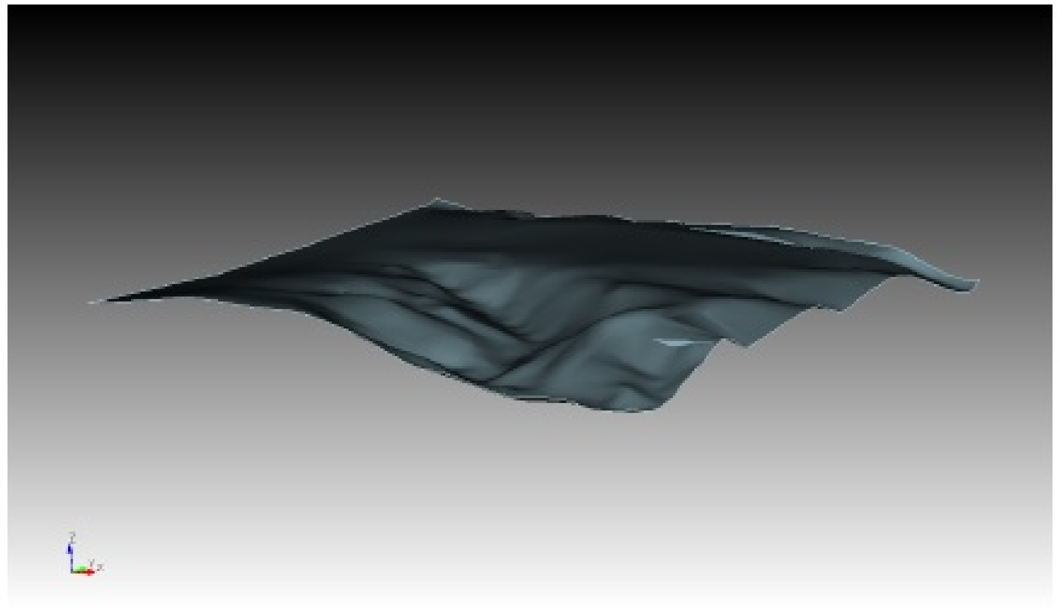
(c) Vertex A3

Finite-element simulations

- Trelis
- SPECFEM3D Cartesian
- Convolutional perfectly matched layer (C-PML)

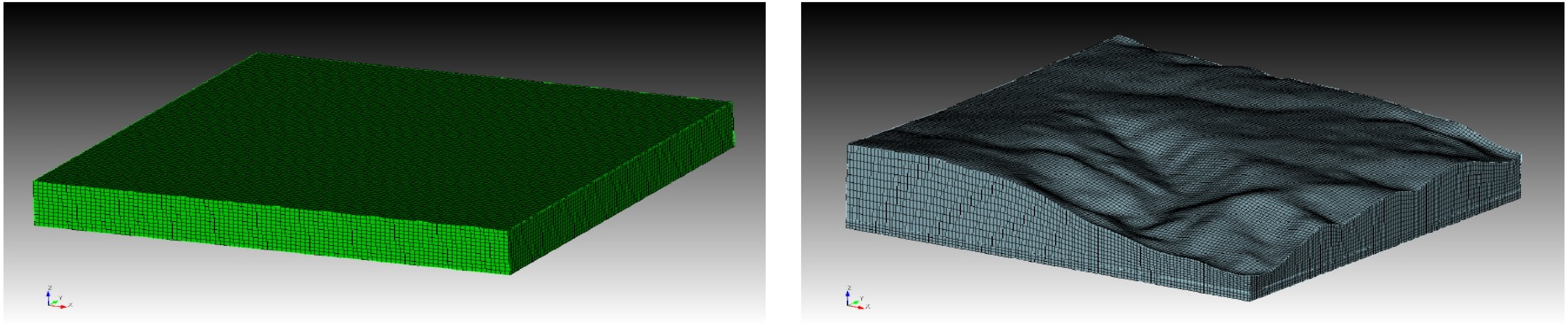

(a) Flat (b) Topography

Meshed models

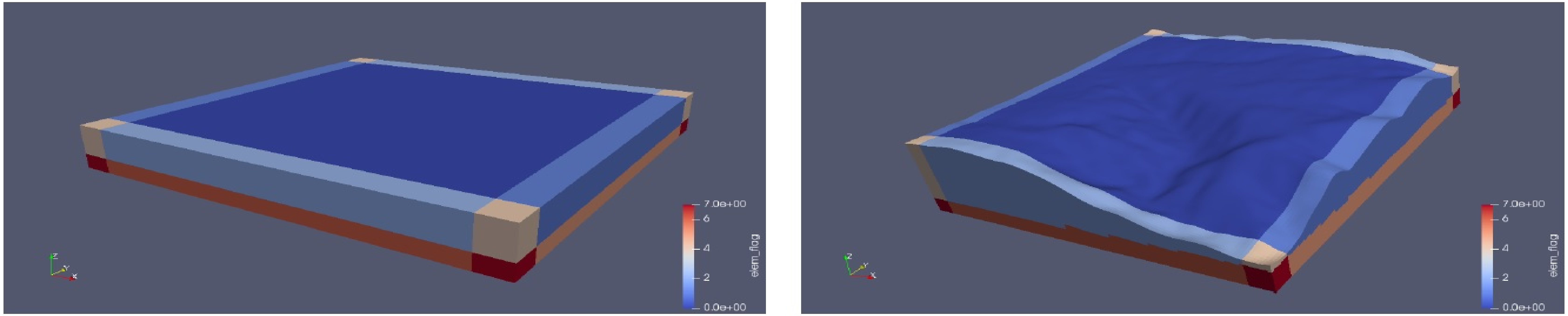

(a) Flat (b) Topography (A3)

Models with C-PML

Results

- Seismic coherence $$c_{ij}(f) = \frac{S_{ij}(f)}{\sqrt{S_i(f)S_j(f)}}$$

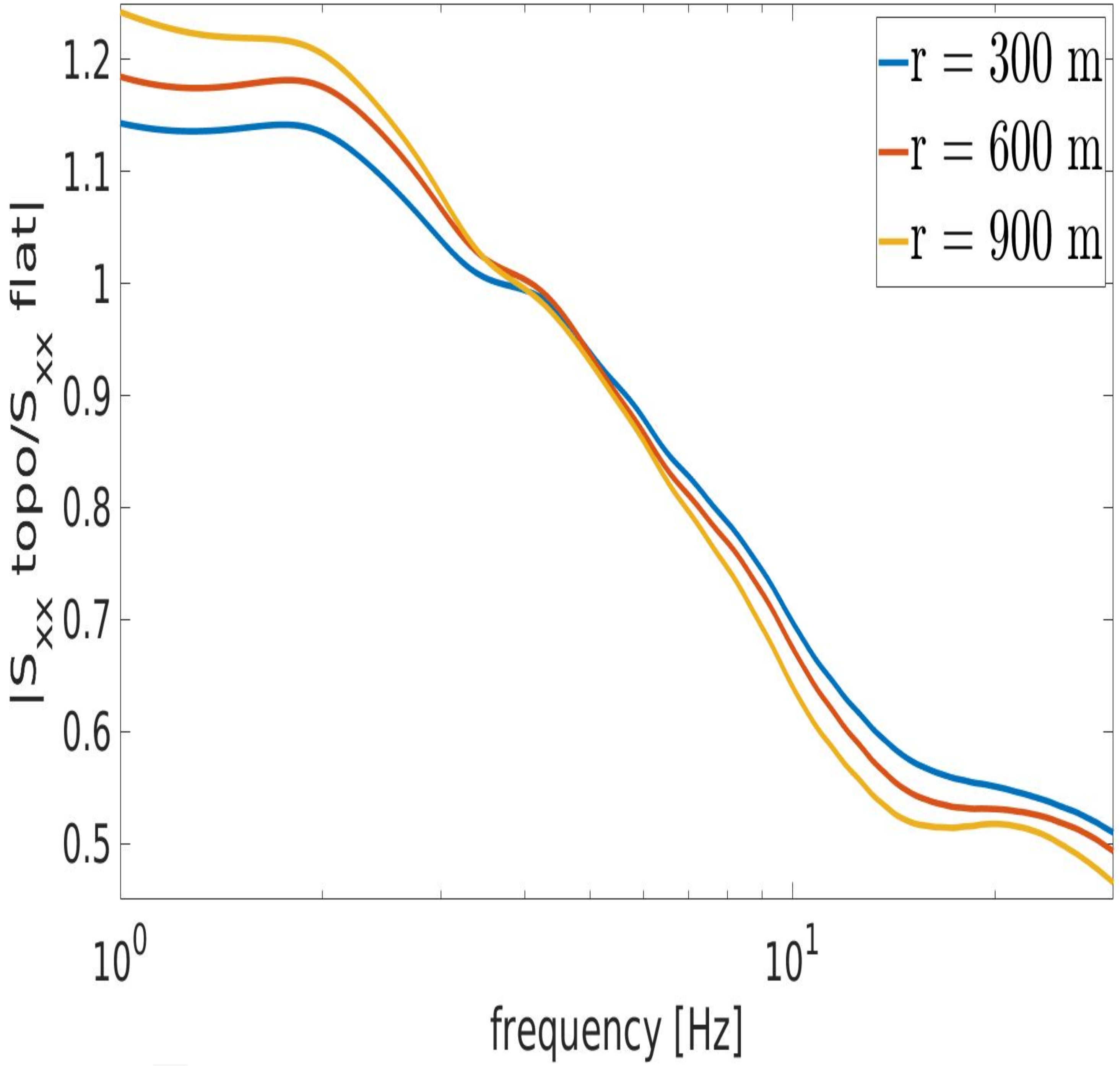

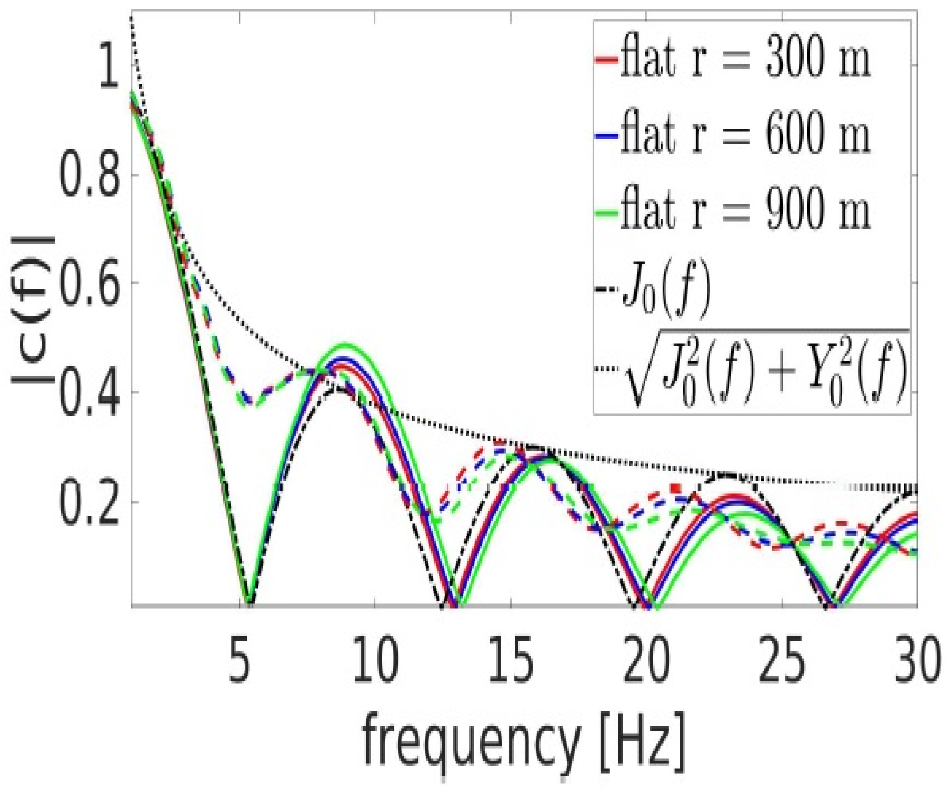

(a) Varying sizes of source-exclusion zones.

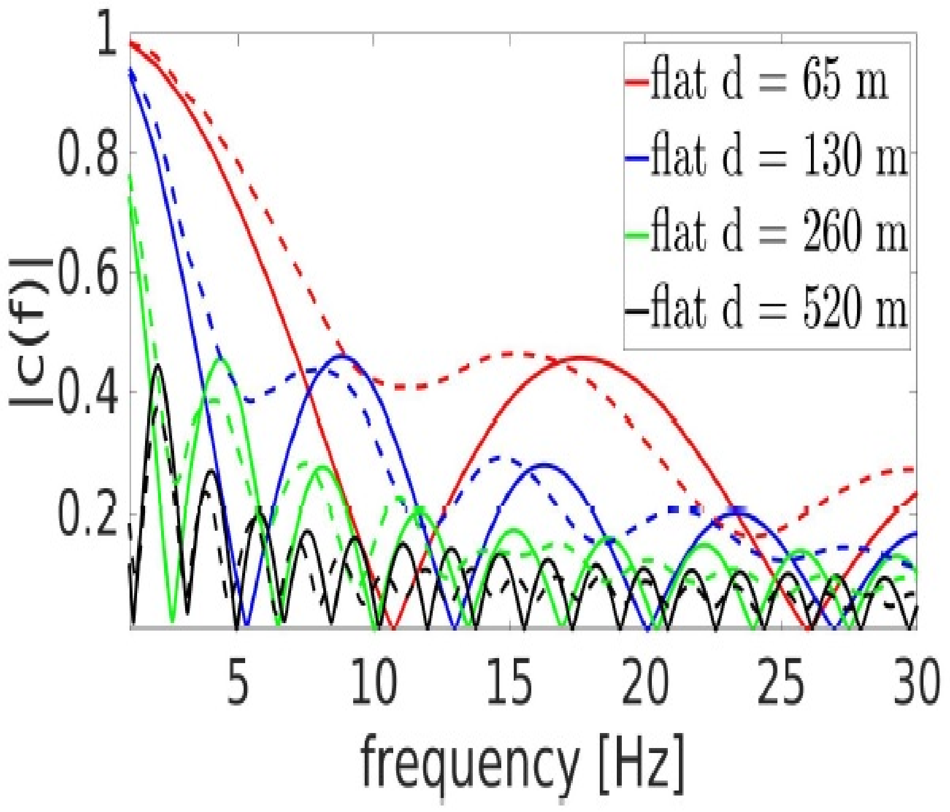

(b) Varying distances between receivers.

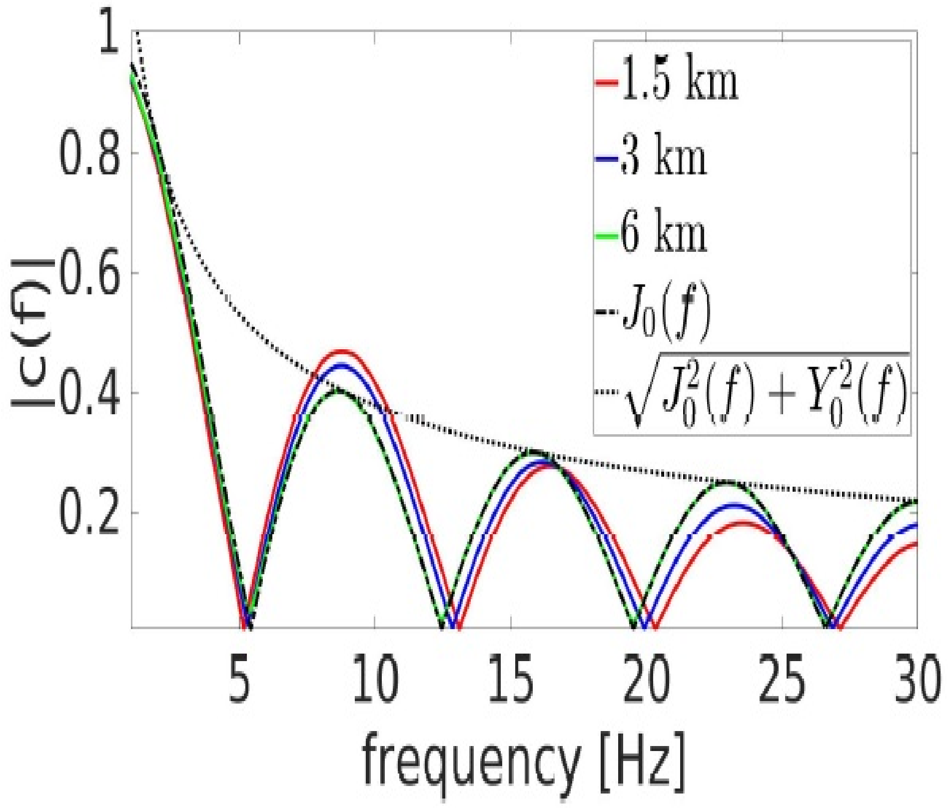

(c) Varying FEM sizes.

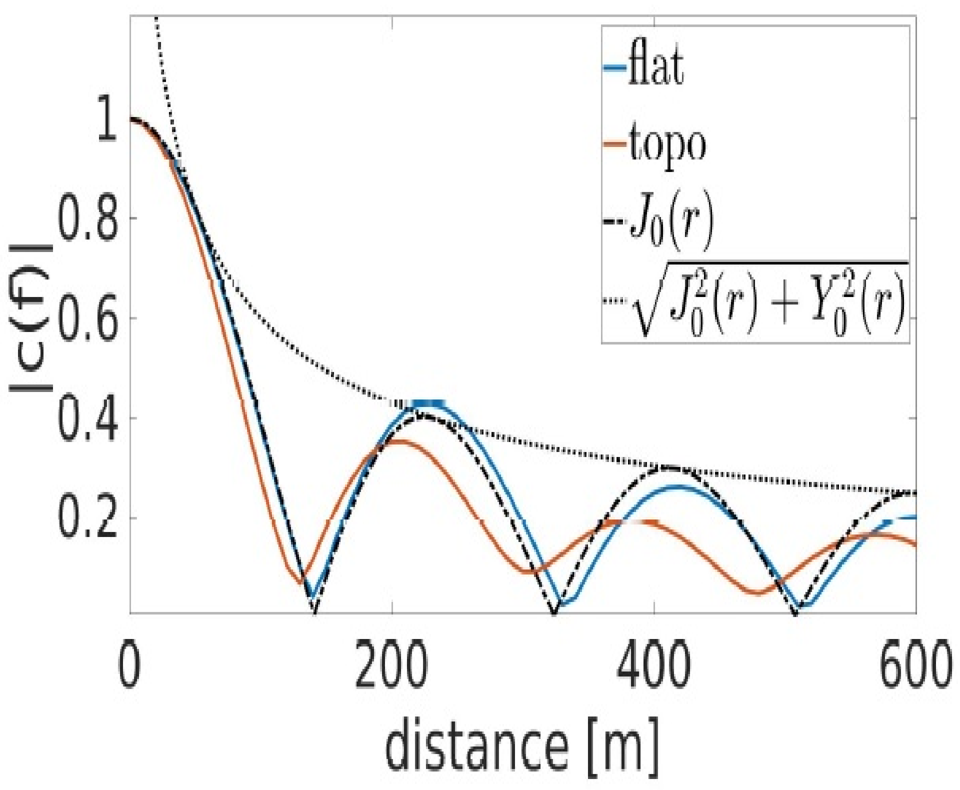

(d) As a function of distance at 5 Hz.

Results

- Seismic correlations

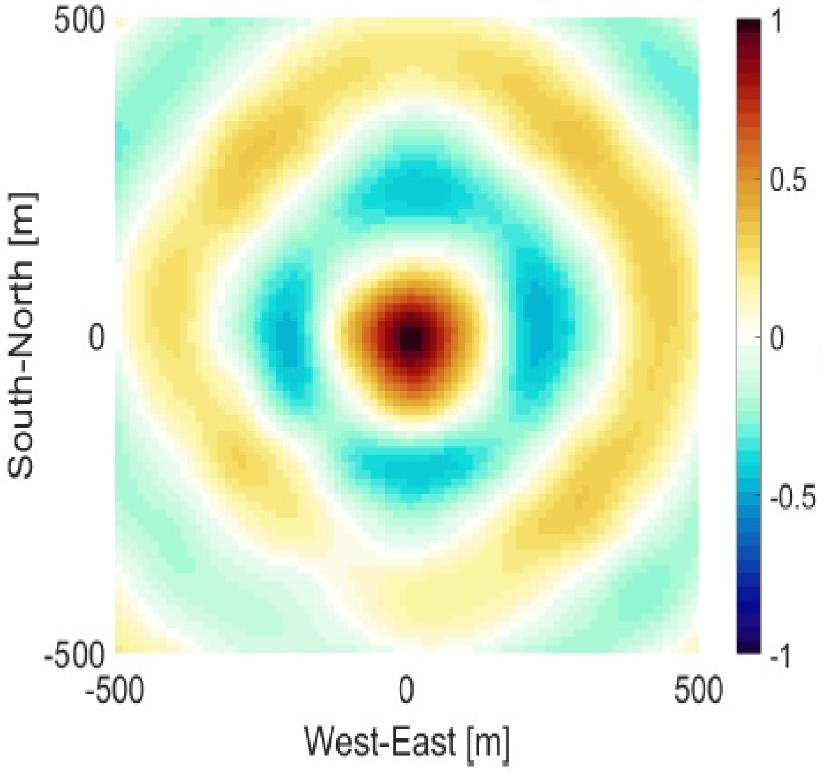

(a) SPECFEM3D simulation.

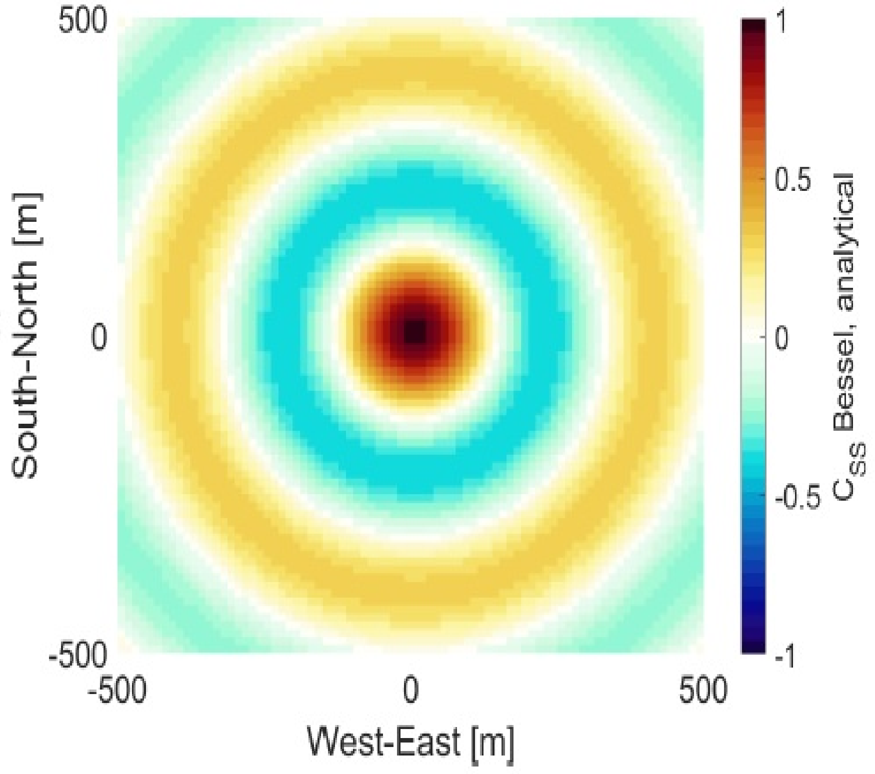

(b) Flat-surface, isotropic.

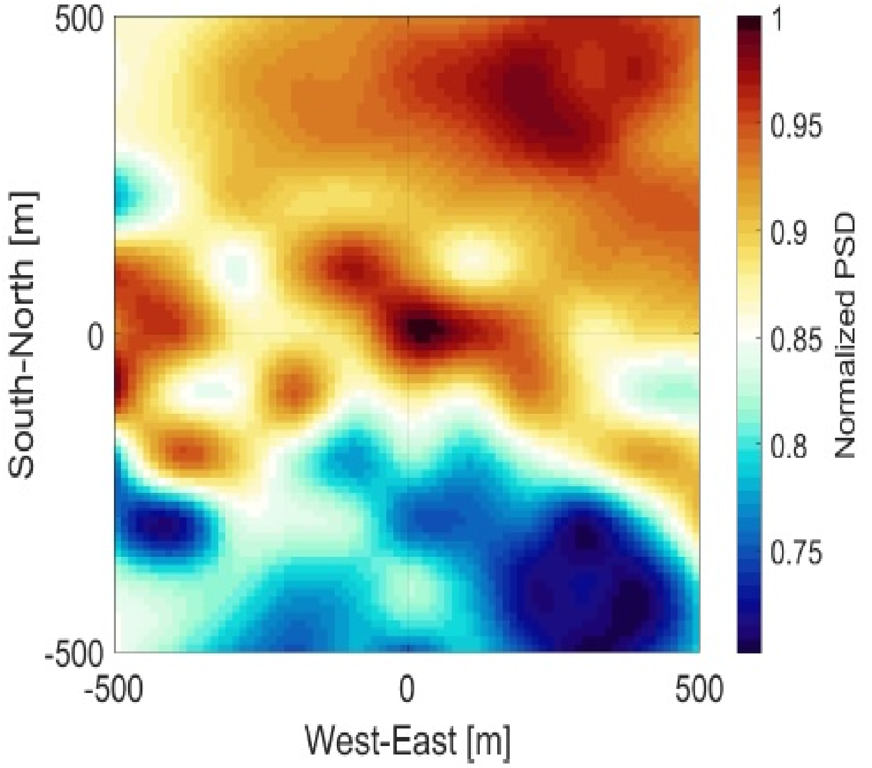

(c) Simulated vertical seismic displacement.

- Gravity-displacement correlations

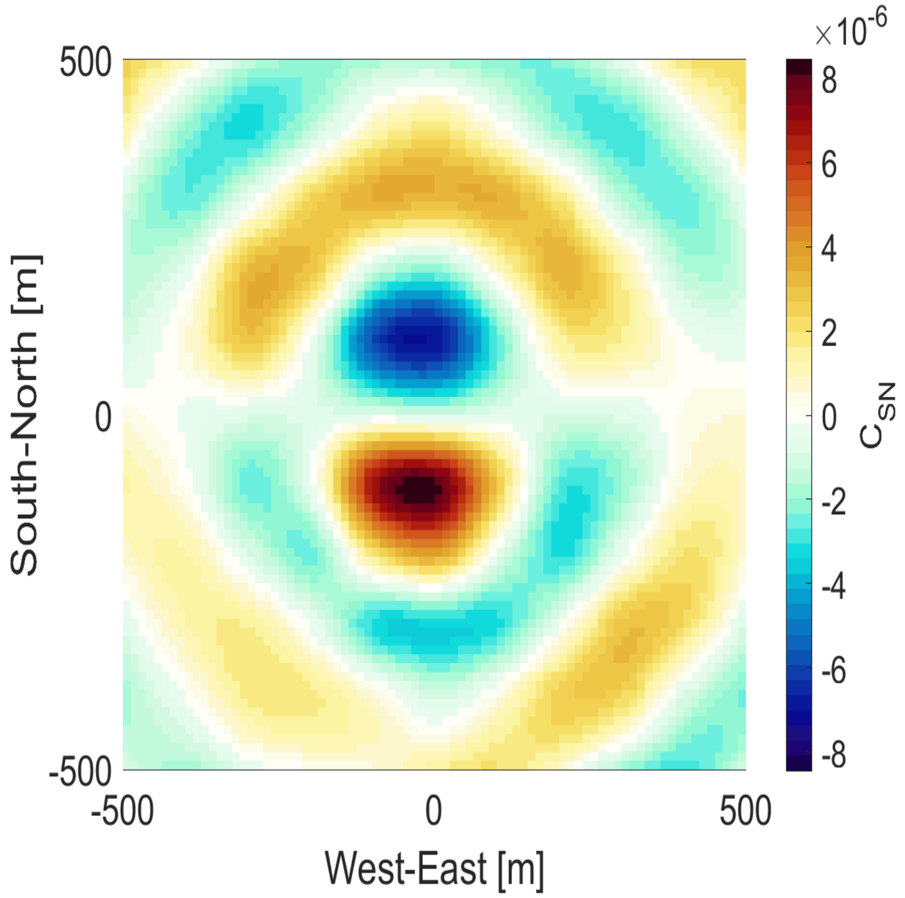

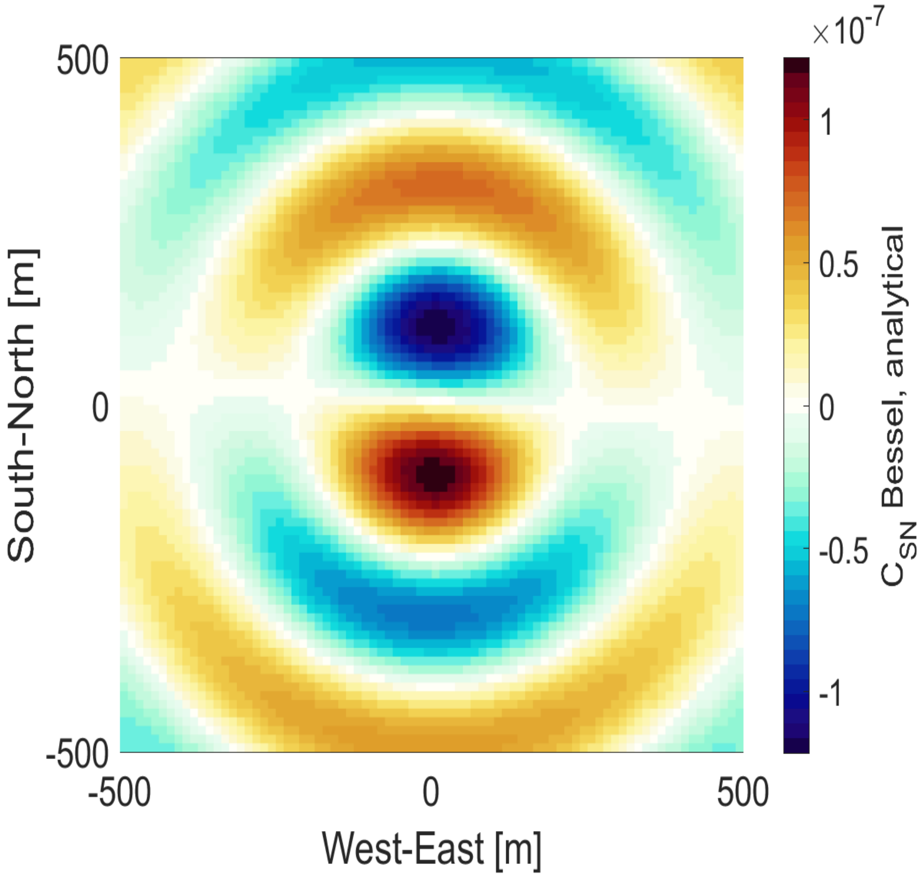

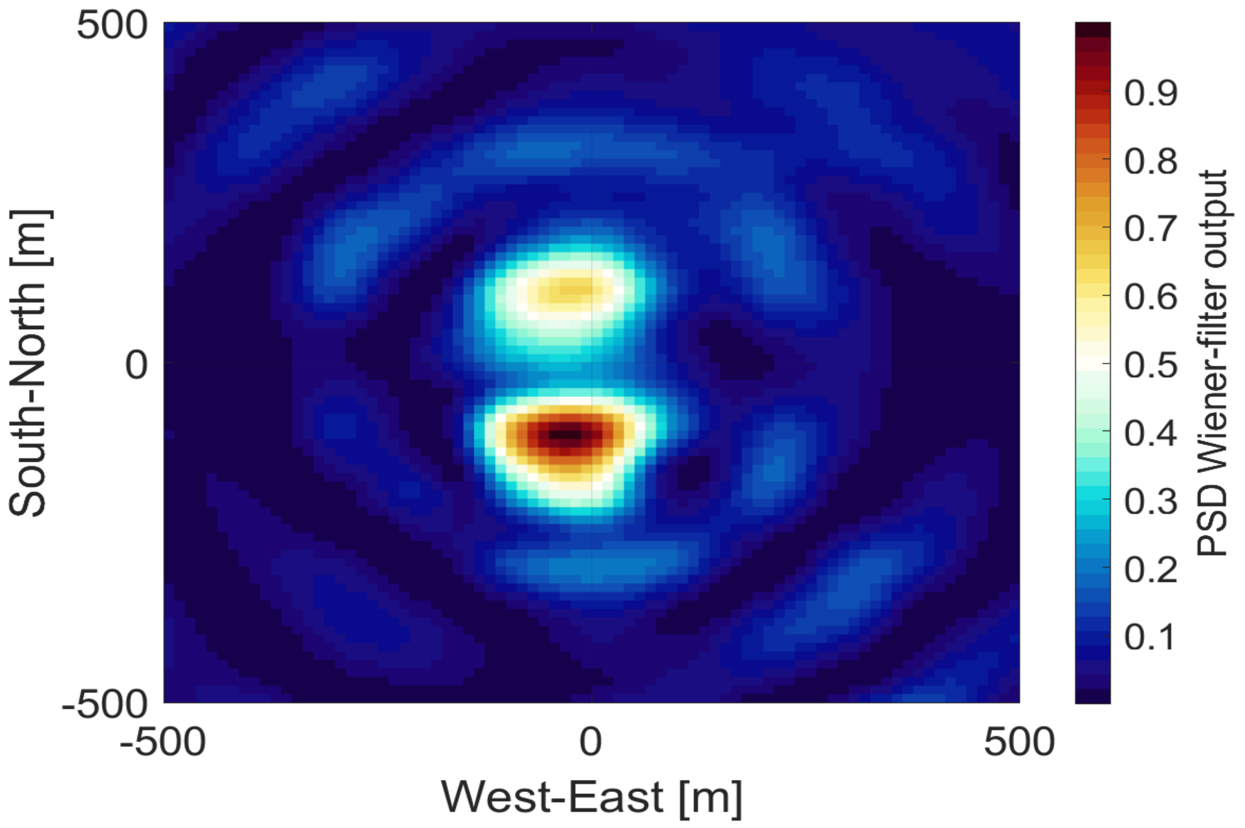

Significance

- Estimates of gravitoelastic correlations - optimization of surface arrays
- Effects of topography on correlations and NN cancellation

- Important milestone, but only one step in a series of tasks:
  1. Include the remaining two contributions in simulations of seismic correlations
  2. Measure seismic correlations at Sardinia site
  3. Simulation + measurement – to improve the estimation of seismic correlations
  4. Multi-sensor numerical optimization routines

- Importance:
  1. Decrease the required effort and therefore cost of a NN mitigation system
  2. Optimal arrays for the best NN reduction – increased sensitivity

JGR Solid Earth

Research Article

Simulations of gravitoelastic correlations for the Sardinian candidate site of the Einstein Telescope

Tomislav Andric, Jan Harms

First published: 28 September 2020 | https://doi.org/10.1029/2020JB020401

Abstract

Gravity fluctuations produced by ambient seismic fields are predicted to limit the sensitivity of the next-generation, gravitational-wave detector Einstein Telescope at frequencies below 20 Hz. The detector will be hosted in an underground infrastructure to reduce seismic disturbances and associated gravity fluctuations. Additional mitigation might be required by monitoring the seismic field and using the data to estimate the associated gravity fluctuations and to subtract the estimate from the detector data, a technique called coherent noise cancellation. In this paper, we present a calculation of correlations between surface displacement of a seismic field and the associated gravitational fluctuations using the spectral-element SPECFEM3D Cartesian software. The model takes into account the local topography at a candidate site of the Einstein Telescope at Sardinia. This paper is a first demonstration of SPECFEM3D's capabilities to provide estimates of gravitoelastic correlations, which are required for an optimized deployment of seismometers for gravity-noise cancellation.

https://agupubs.onlinelibrary.wiley.com/doi/10.1029/2020JB020401

https://www.essoar.org/doi/abs/10.1002/essoar.10503439.2

Alignment sensing and control

- QUAD – LIGO

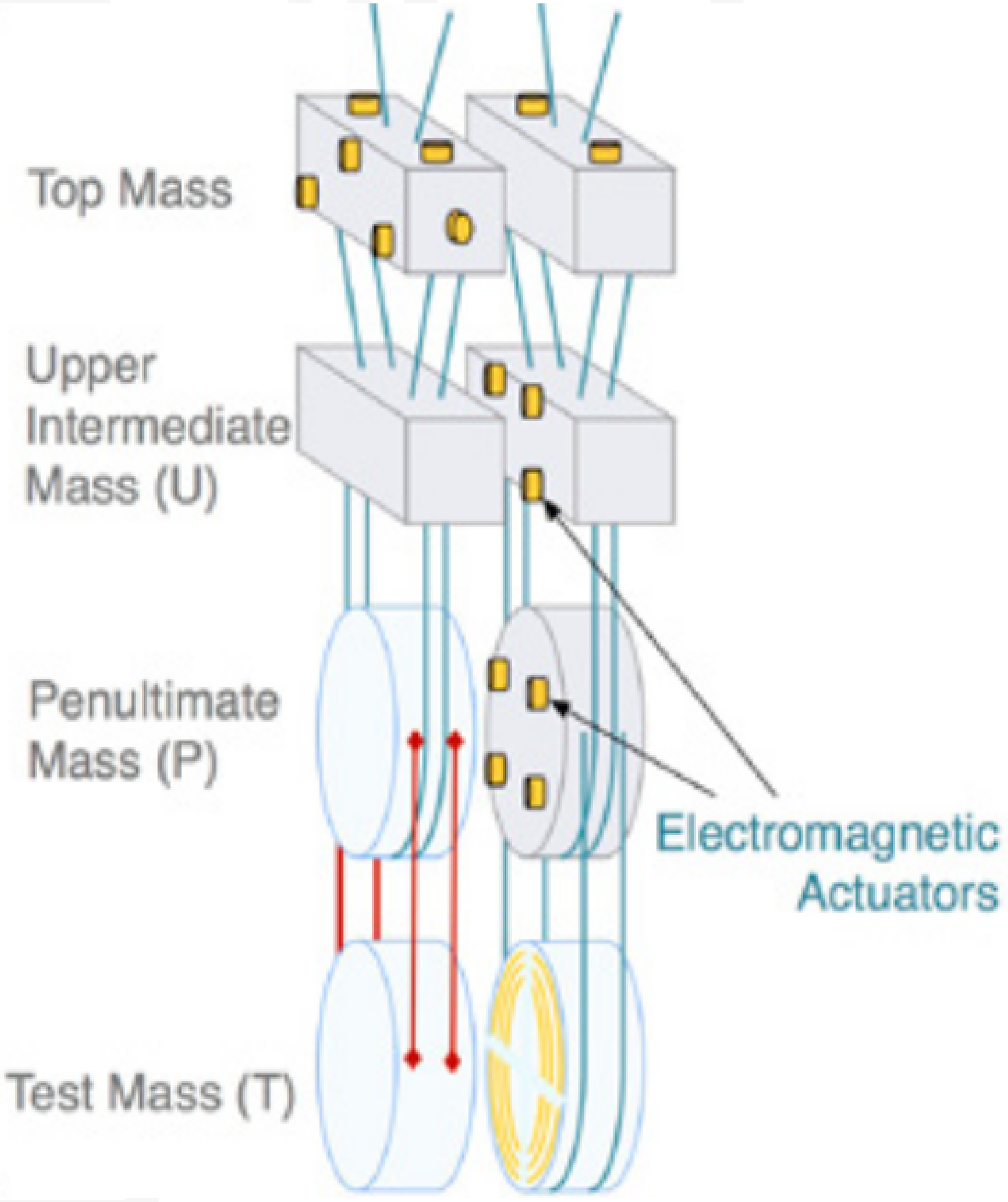

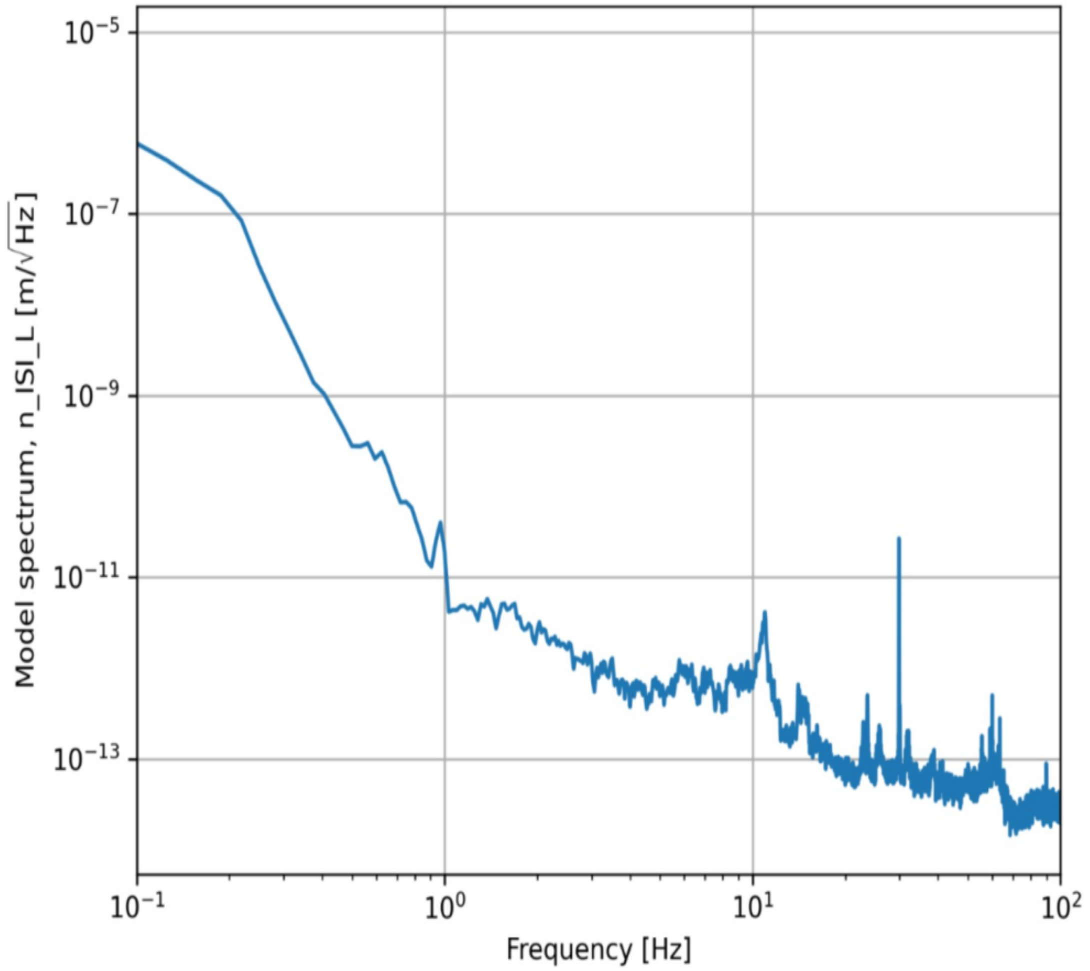

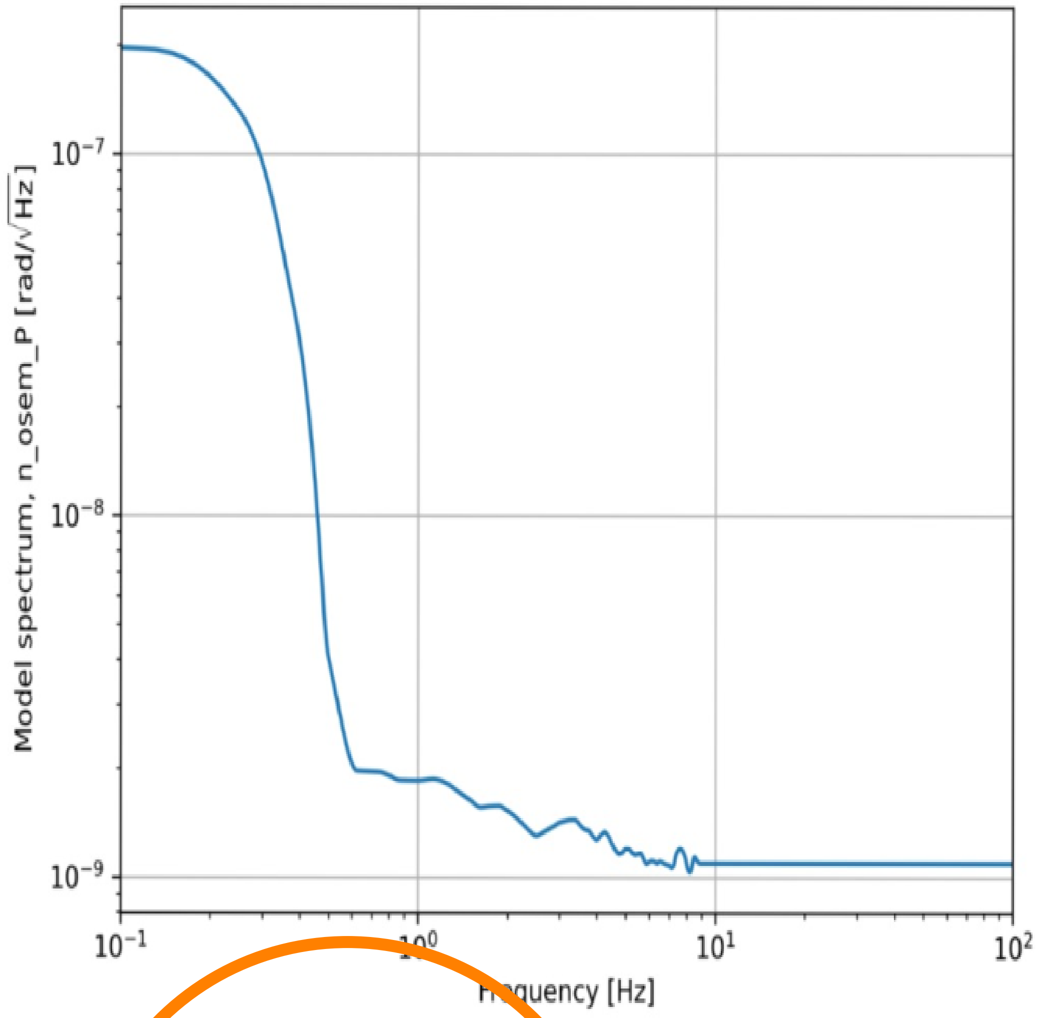

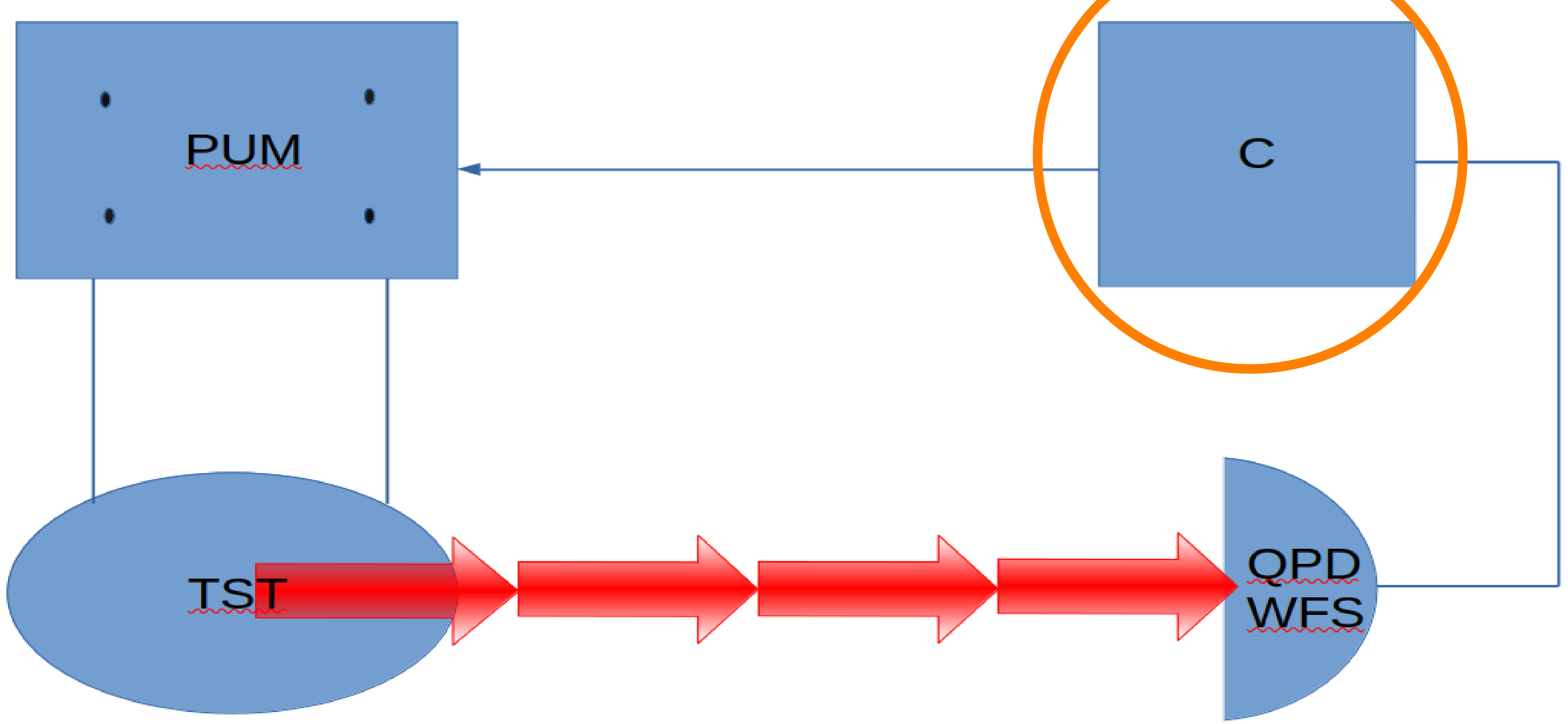

Alignment sensing and control

- Requirements:
  1. 1 nrad RMS
  2. Lowest possible noise above 10 Hz

- LIGO – limited by ASC noise
- No straight-forward solution
- ET – issue needs to be addressed already with its design
- Low light power, increased mass of TM (reduce the angular optomechanical instabilities)

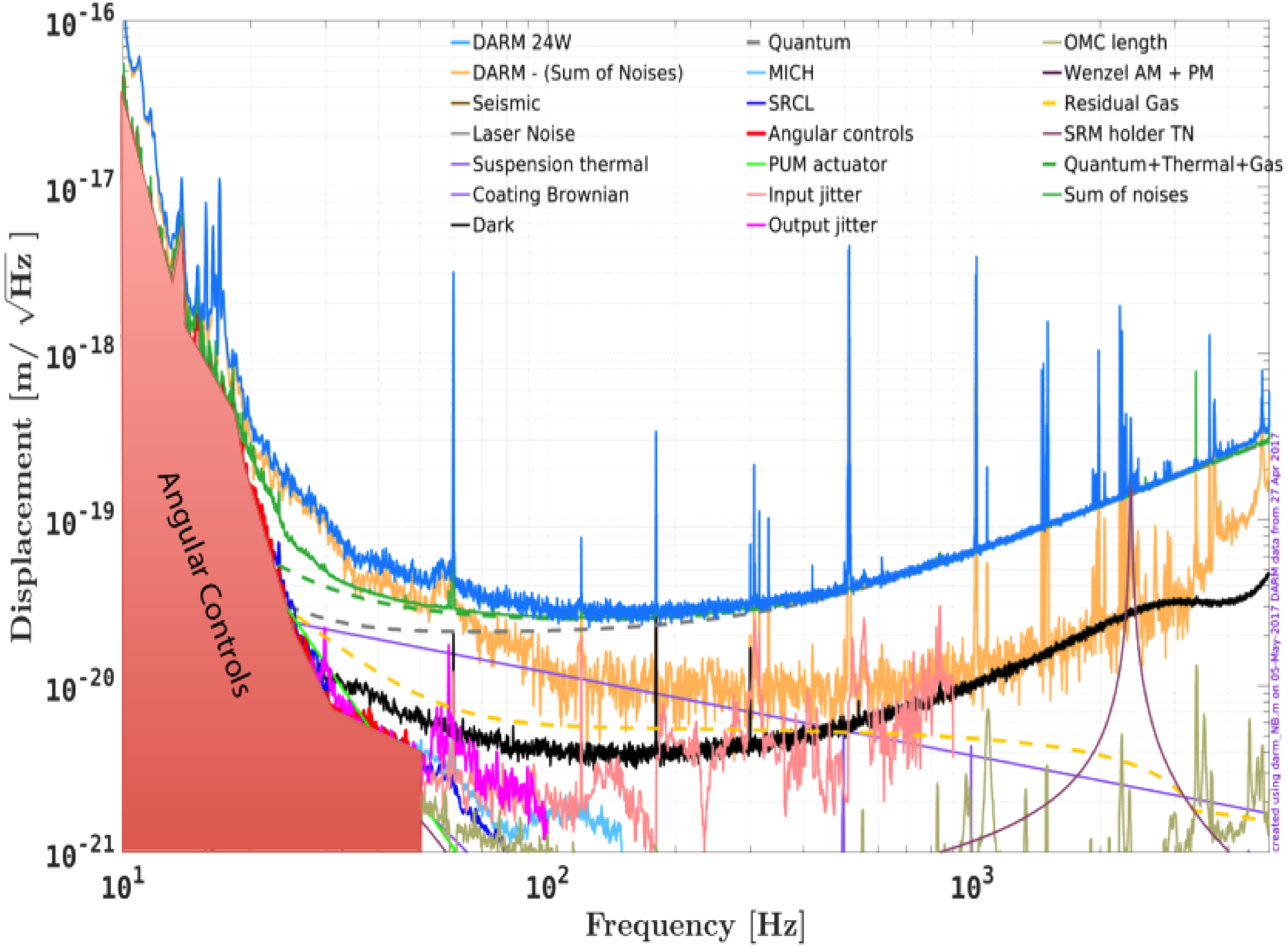

Alignment sensing and control

- Time domain simulations of the ASC
- Currently feedback is done by linear filter designed by commissioners
- ML to improve our feedback control (nonlinear filter that substitutes ASC control; will be developed and tested with the time-domain simulations)
- Caltech 40m prototype - first experimental test
- Implement more accurate A2L coupling and simulate noise

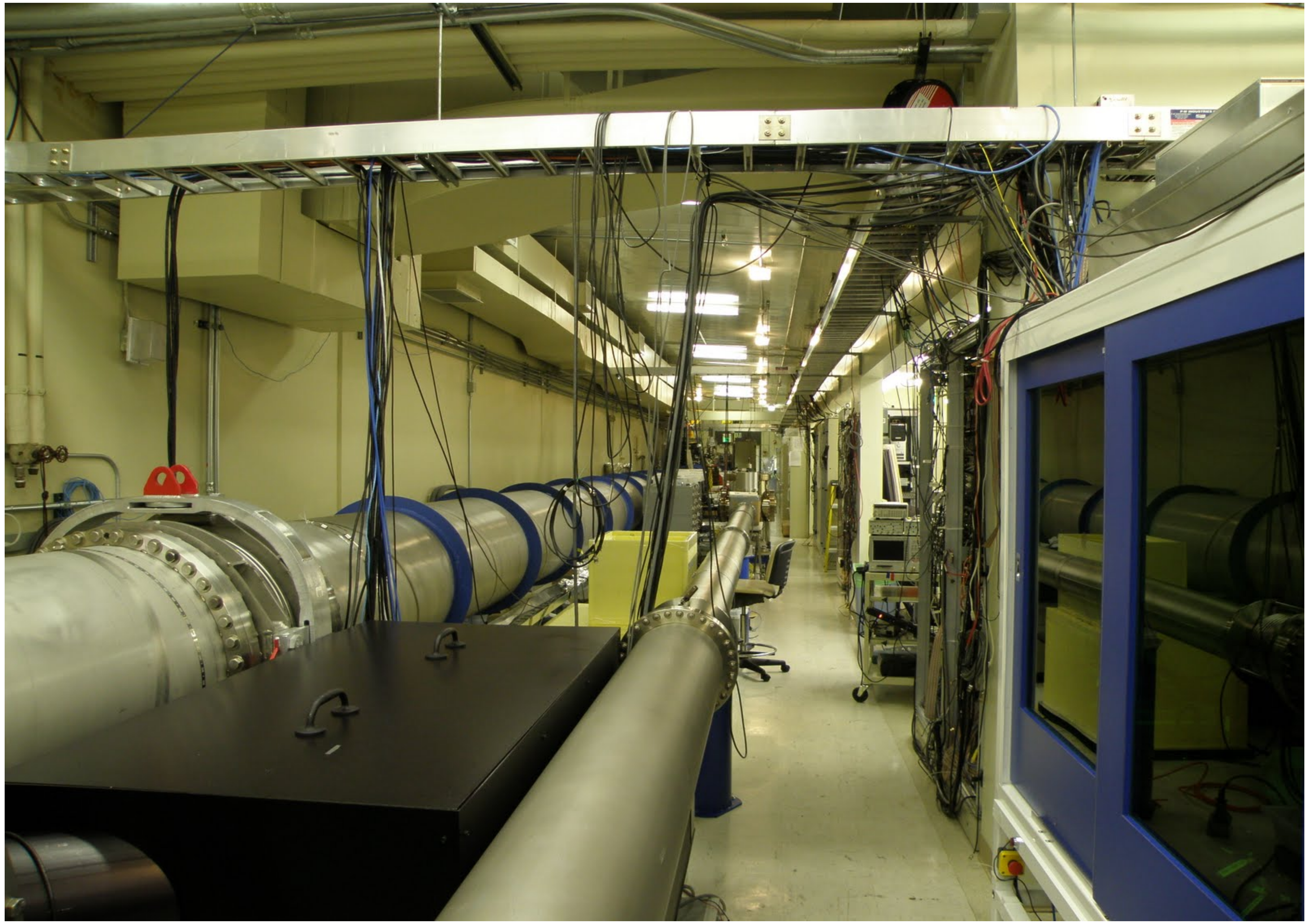

G S
S I

GRAN SASSO
SCIENCE INSTITUTE

Thank you for your attention

www.gssi.it

Backup

It uses a mesh of hexahedral finite elements on which the wave field is represented in terms of high-degree Lagrange polynomials on Gauss–Lobatto–Legendre interpolation points.

For cross-correlation simulations, the distribution of noise sources in SPECFEM3D Cartesian is constrained to the surface, which is not a major drawback since the most relevant seismic sources in the NN band are expected to be surface sources.

The source-time function of the generating wavefield is obtained using the spectrum of the ensemble-averaged noise, and it is narrowly concentrated around zero time. We use a source-time function shown in figure 6a representing a frequency-independent seismic spectrum in the interesting frequency range (1 – 30 Hz), since the absolute values of the seismic spectrum are not relevant for this paper. Generally, results in frequency domain can be rescaled using realistic / observed seismic spectra when needed.

We used Trelis for the creation of models and their exporting into a SPECFEM3D Cartesian file format. Trelis is a full-featured software for generation of two- and three-dimensional finite-element grids (meshes) and geometry preparation

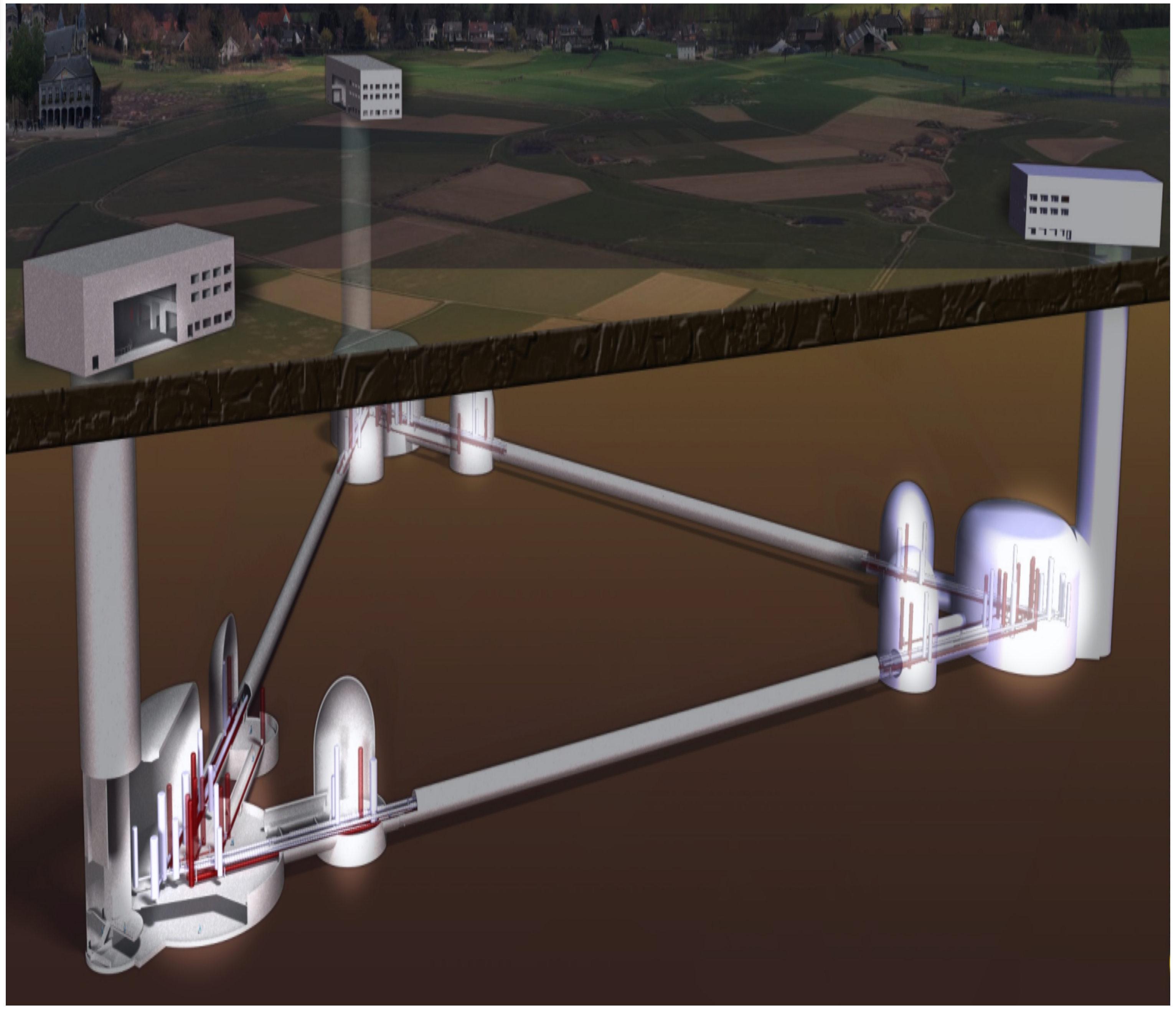

One of the most important data-processing techniques in all of the ambient-noise seismology is ensemble averaging, allowing to reduce the effects of a set of scatterers and sources randomly distributed in time and space to those of a diffuse wavefield

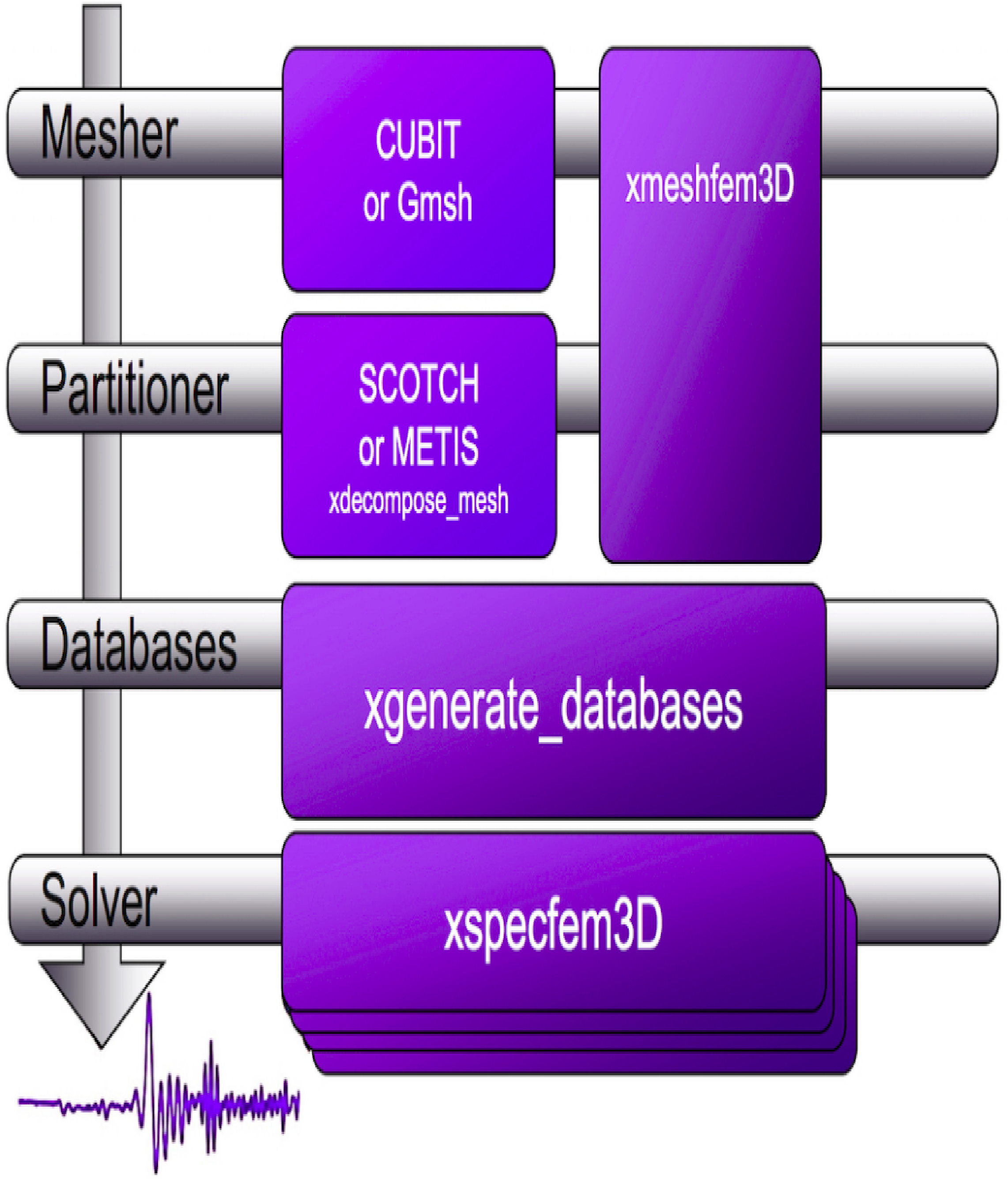

Noise cross-correlation simulations

- Two steps of simulations:
  1. Injection
  2. Noise emission

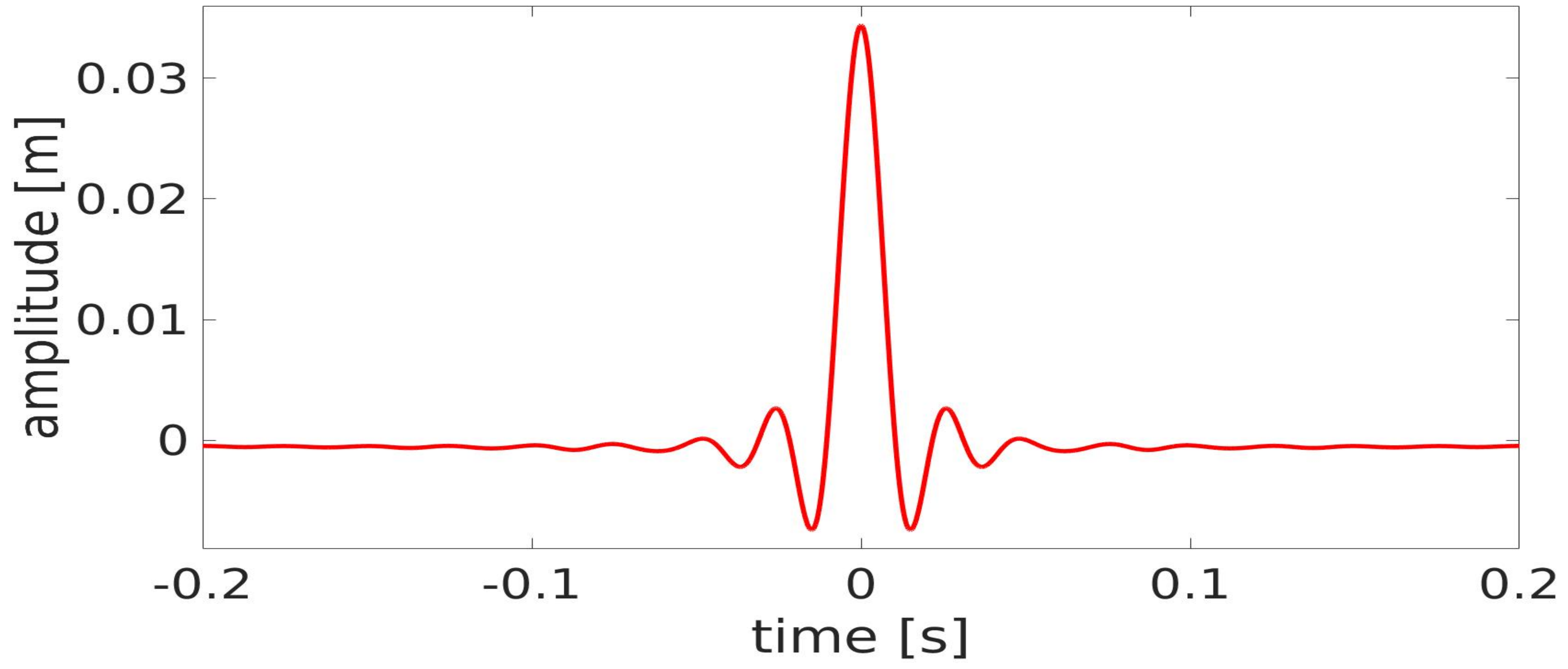

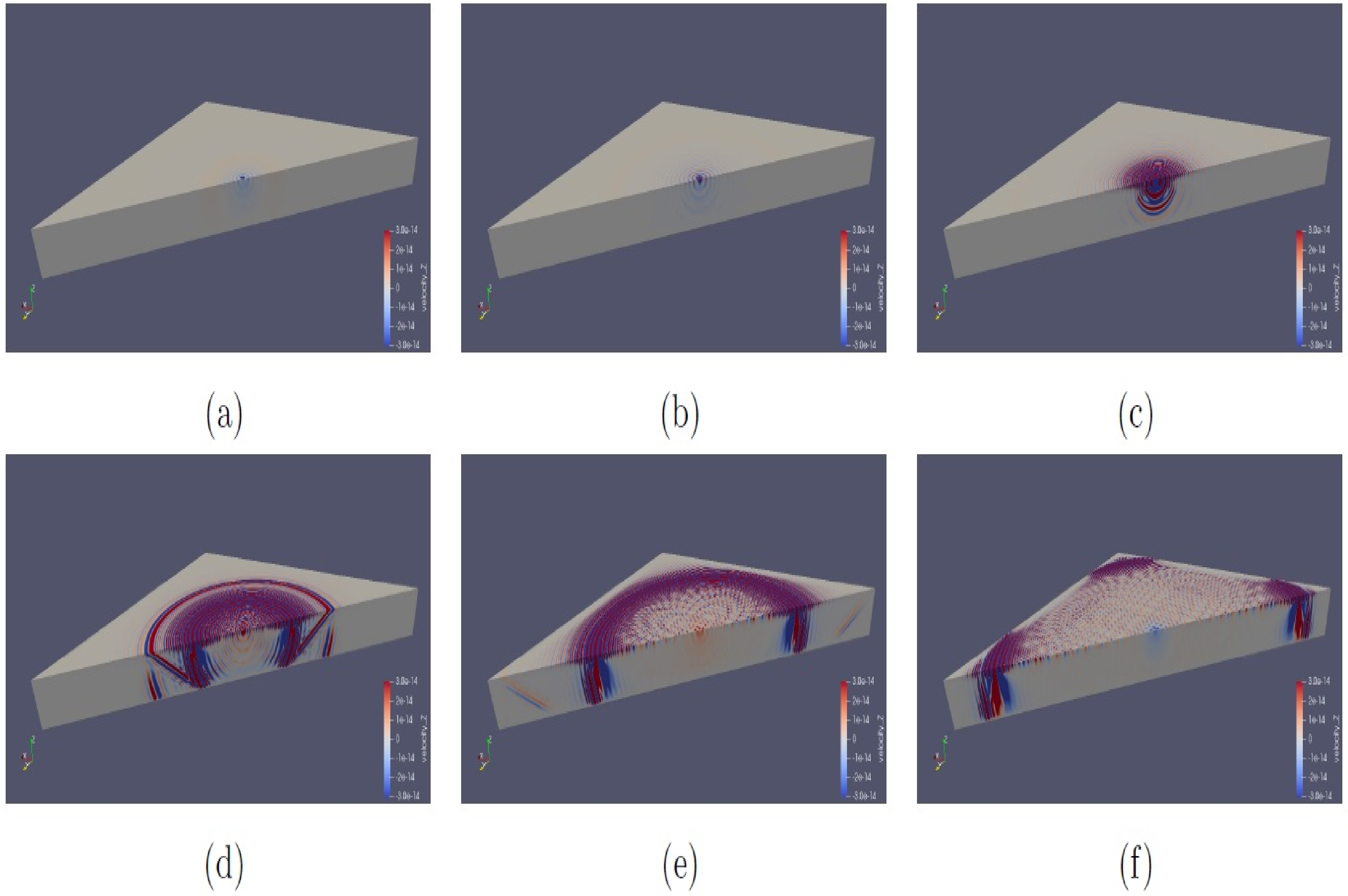
(a) (b) (c)
(d) (e) (f)

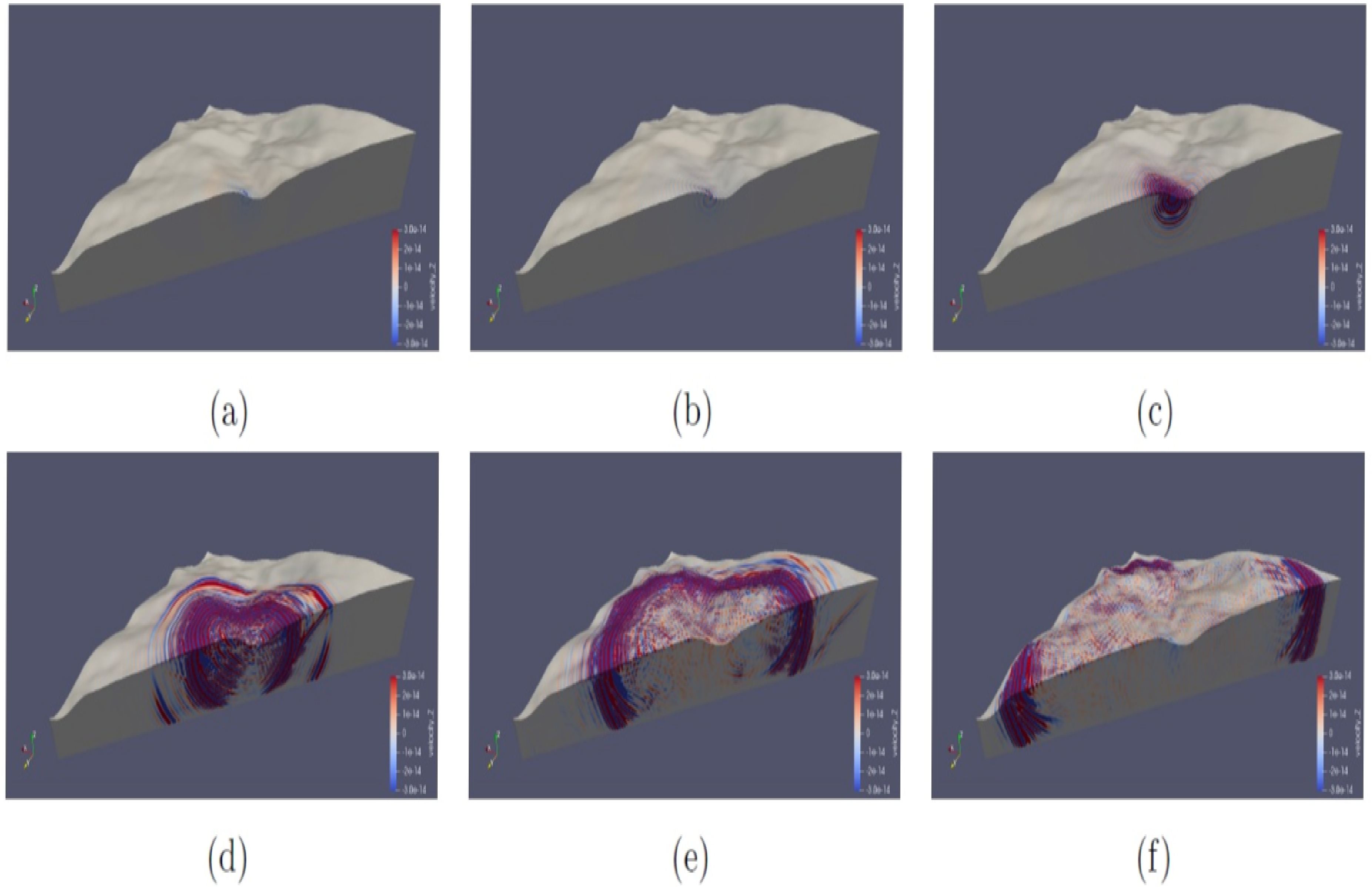
(a) (b) (c)
(d) (e) (f)

Further mitigation of NN can be achieved by noise cancellation using an extensive monitoring system of the ambient seismic field (Harms, 2019). The idea is to pass seismic data through a filter such that its output can be understood as a coherent estimate of seismic NN and be subtracted from the GW data (Cella, 2000)

Nonetheless, the quantities required for such a multi-sensor optimization are provided by SPECFEM3D. They need to be used in numerical optimization routines. What we in fact propose is to use the correlation results from numerical analysis as presented in this paper to define priors for a Gaussian Process Regression, which then combines priors and observed seismic correlations for a Bayesian inference of seismic correlations everywhere in the medium, which forms the basis of the optimization algorithm

As a consequence, and as a first step, we attempt to model the gravitational coupling between seismic surface fields and underground gravitational perturbations.

With the A3-topographic model, |c ij (f)| does not vanish at any frequency, which is likely due to a mixed wave content with Rayleigh waves and scattered waves of different wavelengths

$$C\left(\delta a_{\text{arm}}(\boldsymbol{r}_0), \xi_z(\boldsymbol{r}); f\right) = G\rho_0 \int \mathrm{d}^2\boldsymbol{r}' C\left(\xi_n(\boldsymbol{r}'), \xi_z(\boldsymbol{r}); f\right) \frac{(\boldsymbol{r}' - \boldsymbol{r}_0)\cdot \boldsymbol{e}_{\text{arm}}}{|\boldsymbol{r}' - \boldsymbol{r}_0|^3}$$

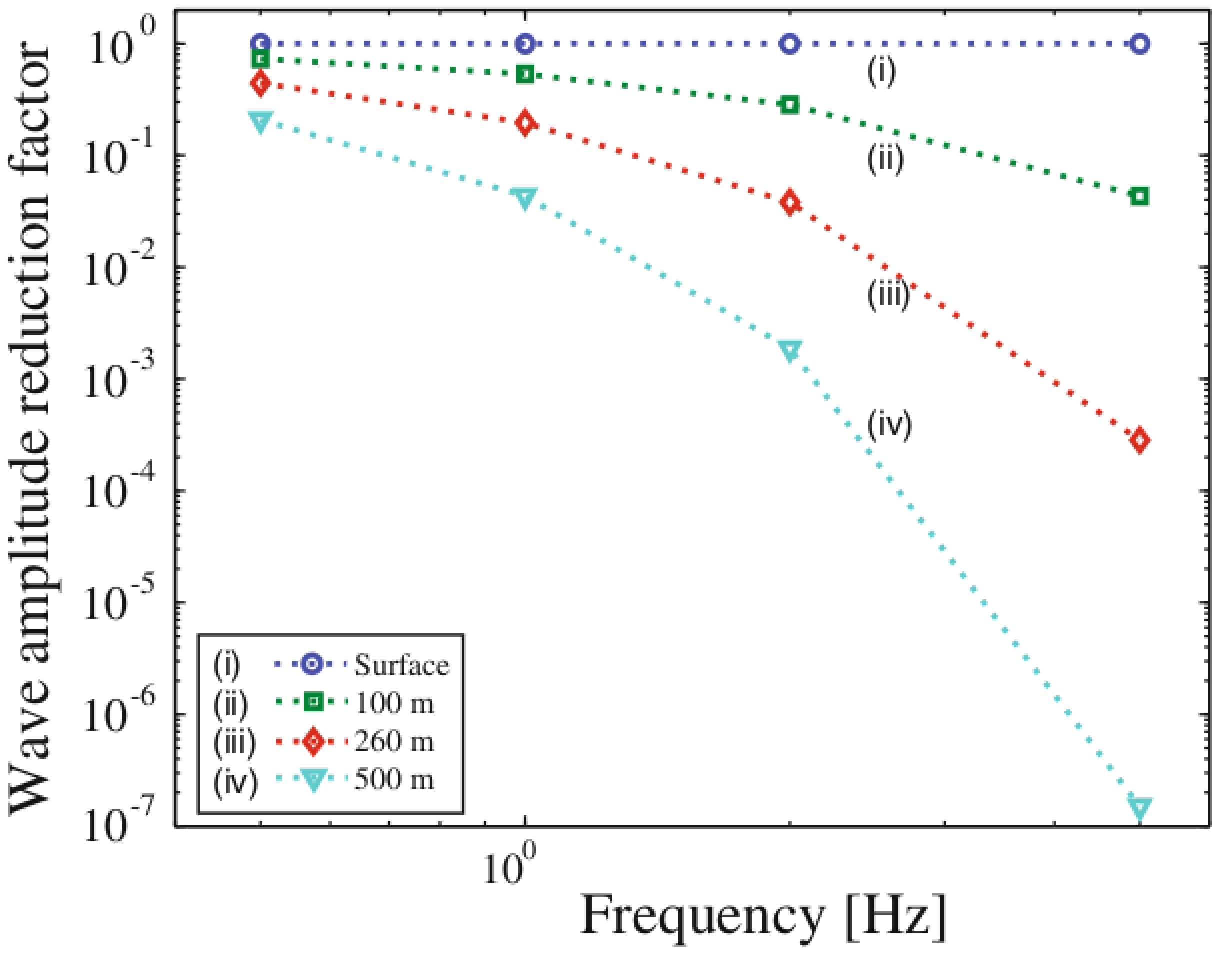

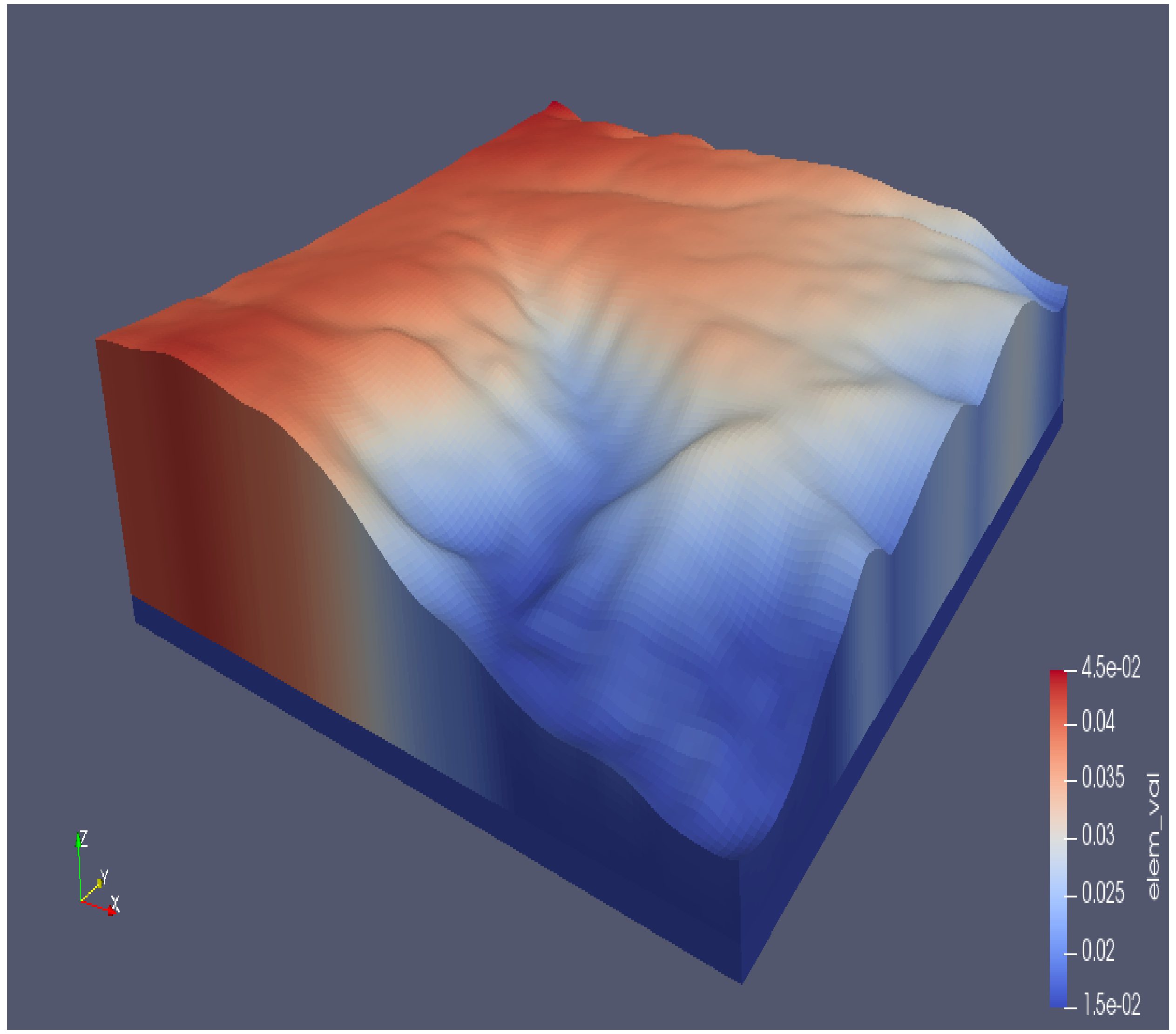

$$C\left(\delta a_{\text{arm}}(0), \xi_z(\boldsymbol{r}); f\right) = 2\pi G\rho_0 S\left(\xi_z; f\right) e^{-hk(f)} \cos(\phi) J_1\left(k(f) r\right),$$

$$S(w; f) = \left|C\left(\delta a_{\text{arm}}(\boldsymbol{r}_0), \xi_z(\boldsymbol{r}); f\right)\right|^2 / C\left(\xi_z(\boldsymbol{r}), \xi_z(\boldsymbol{r}); f\right)$$

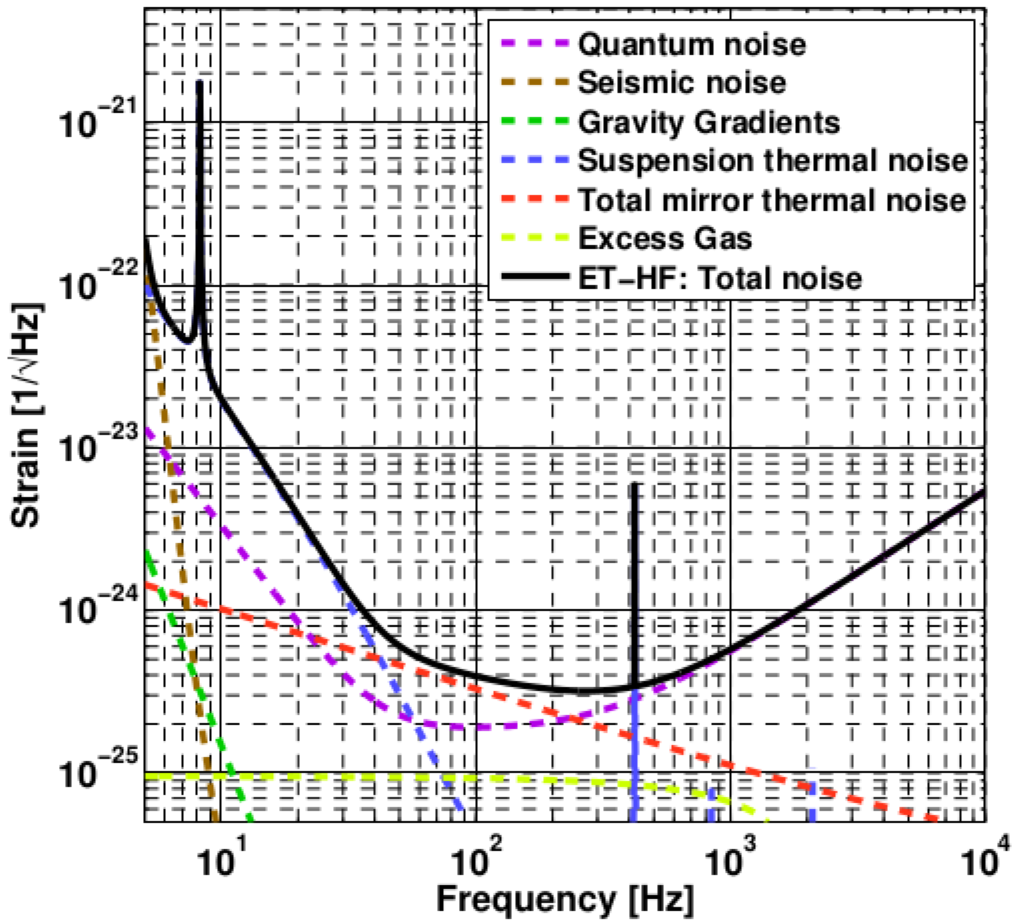
Quantum noise
Seismic noise
Gravity Gradients
Suspension thermal noise
Total mirror thermal noise
Excess Gas
ET–HF: Total noise
Strain [1/√Hz]
10^{-21}
10^{-22}
10^{-23}
10^{-24}
10^{-25}
10^{1}
10^{2}
10^{3}
10^{4}
Frequency [Hz]

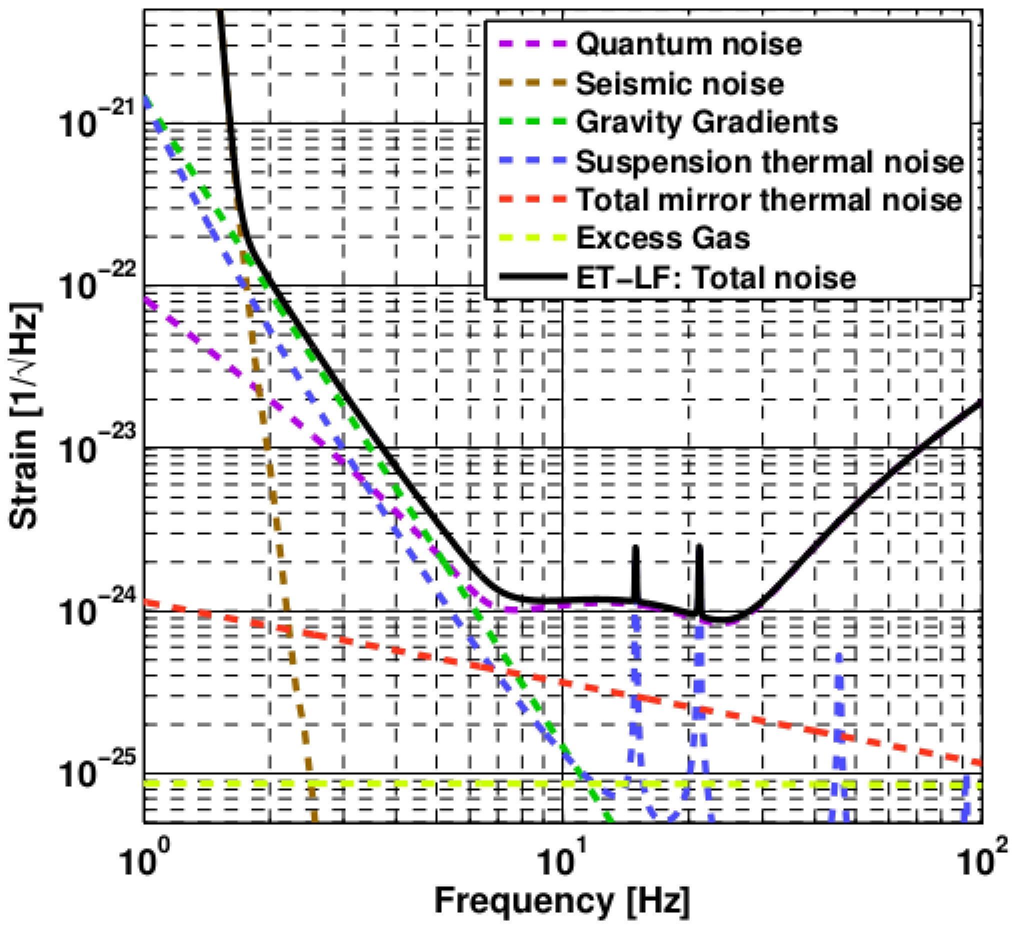
Quantum noise
Seismic noise
Gravity Gradients
Suspension thermal noise
Total mirror thermal noise
Excess Gas
ET–LF: Total noise
Strain [1/√Hz]
10^{-21}
10^{-22}
10^{-23}
10^{-24}
10^{-25}
10^{0}
10^{1}
10^{2}
Frequency [Hz]

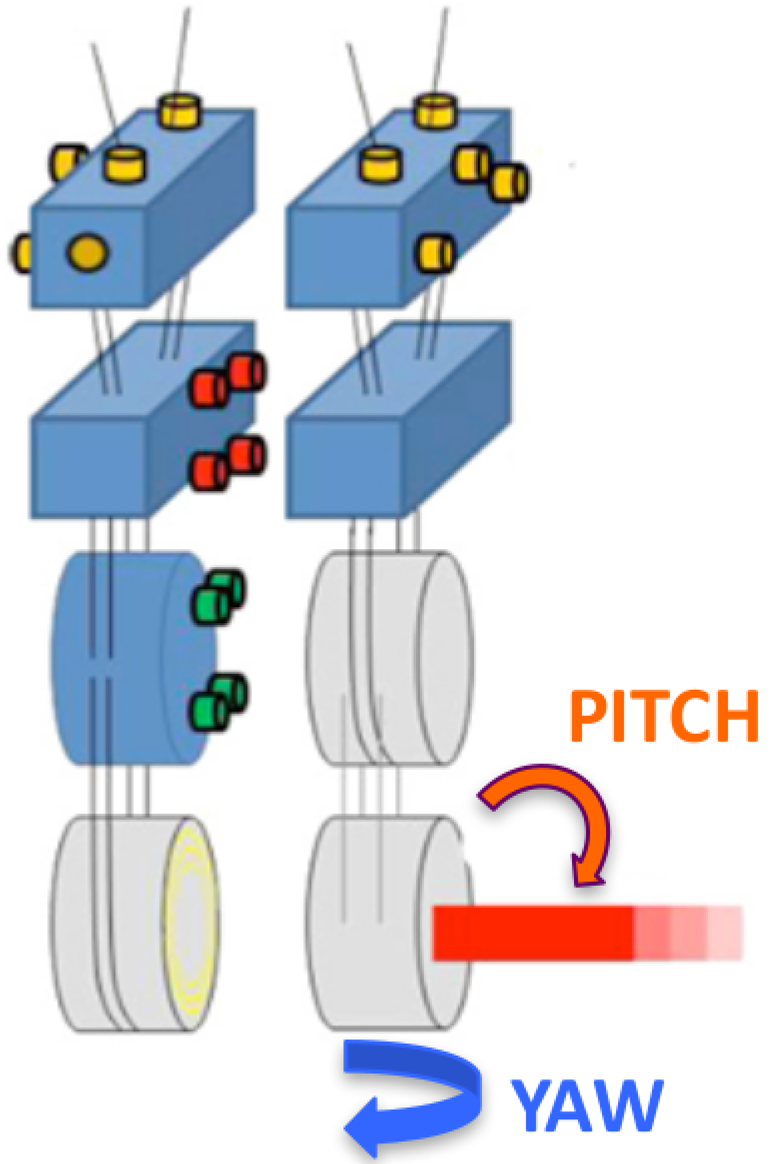
PITCH
YAW

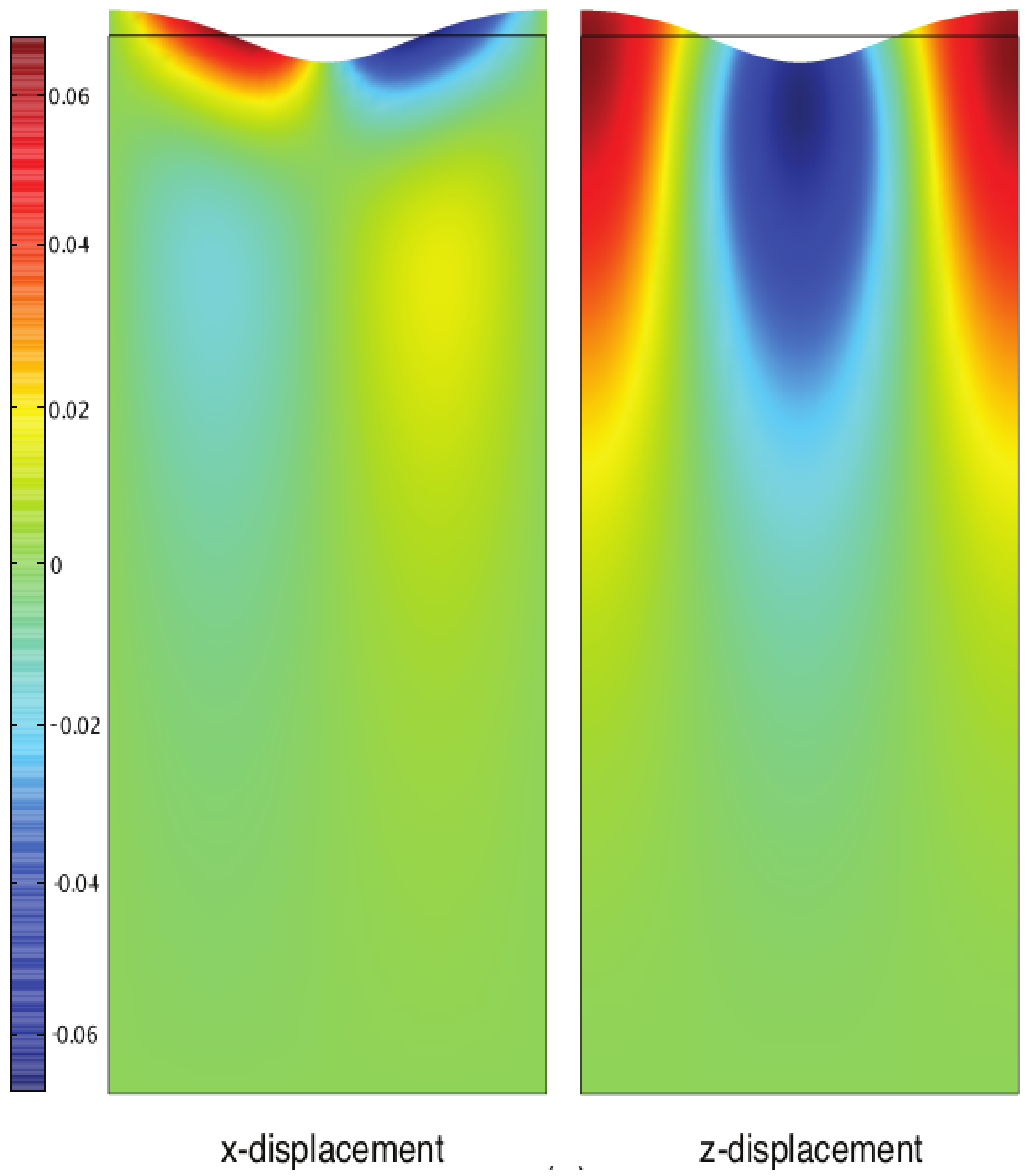
0.06
0.04
0.02
0
-0.02
-0.04
-0.06
x-displacement
z-displacement

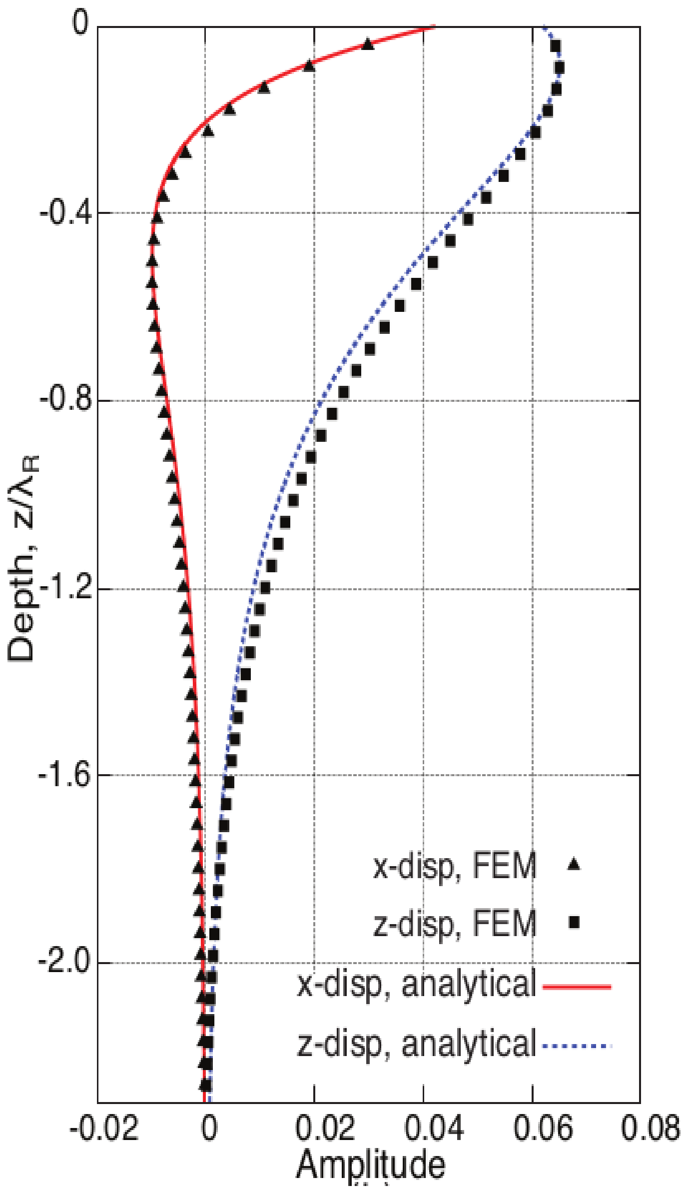
0
-0.4
-0.8
-1.2
-1.6
-2.0
Depth, z/λ_R
x-disp, FEM
z-disp, FEM
x-disp, analytical
z-disp, analytical
-0.02
0
0.02
0.04
0.06
0.08
Amplitude

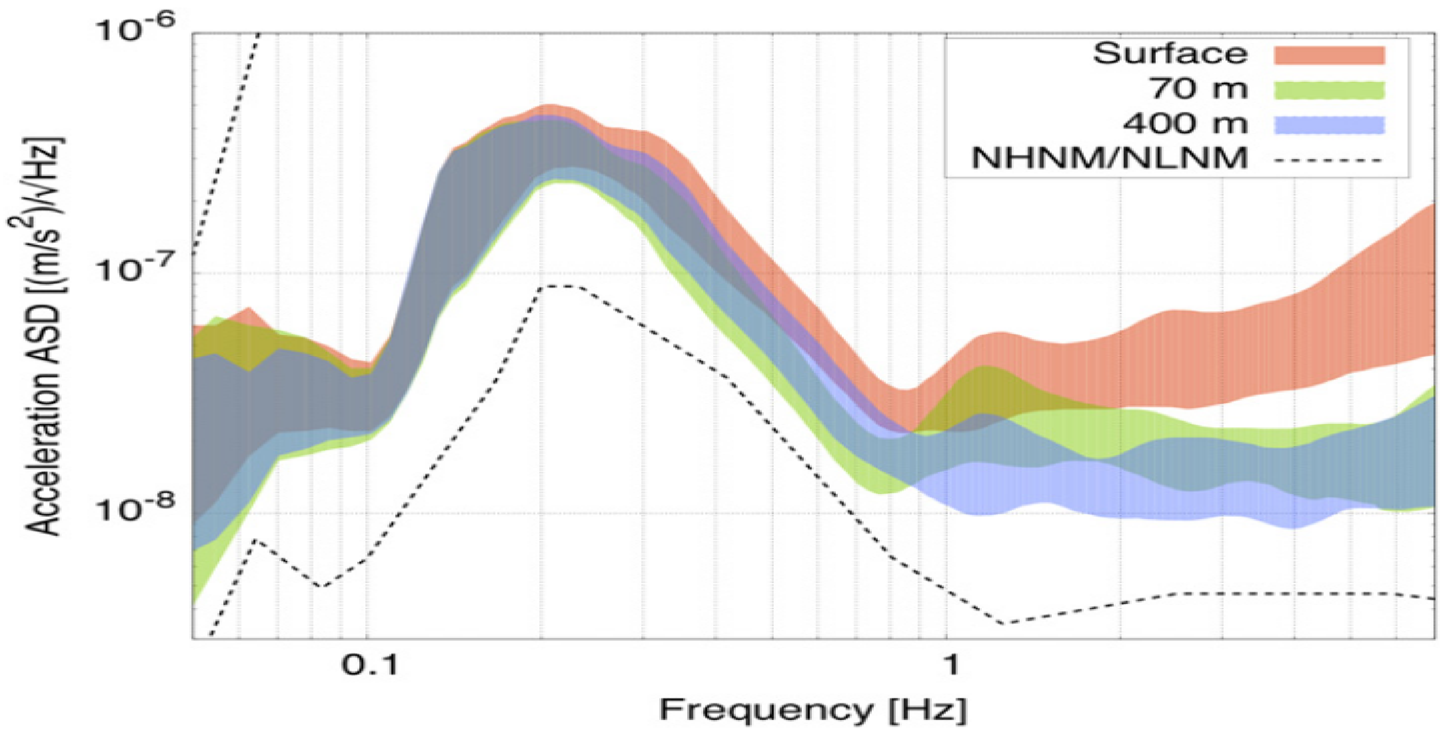
Surface
70 m
400 m
NHNM/NLNM
10^{-6}
10^{-7}
10^{-8}
Acceleration ASD [(m/s^2)/√Hz]
0.1
1
Frequency [Hz]

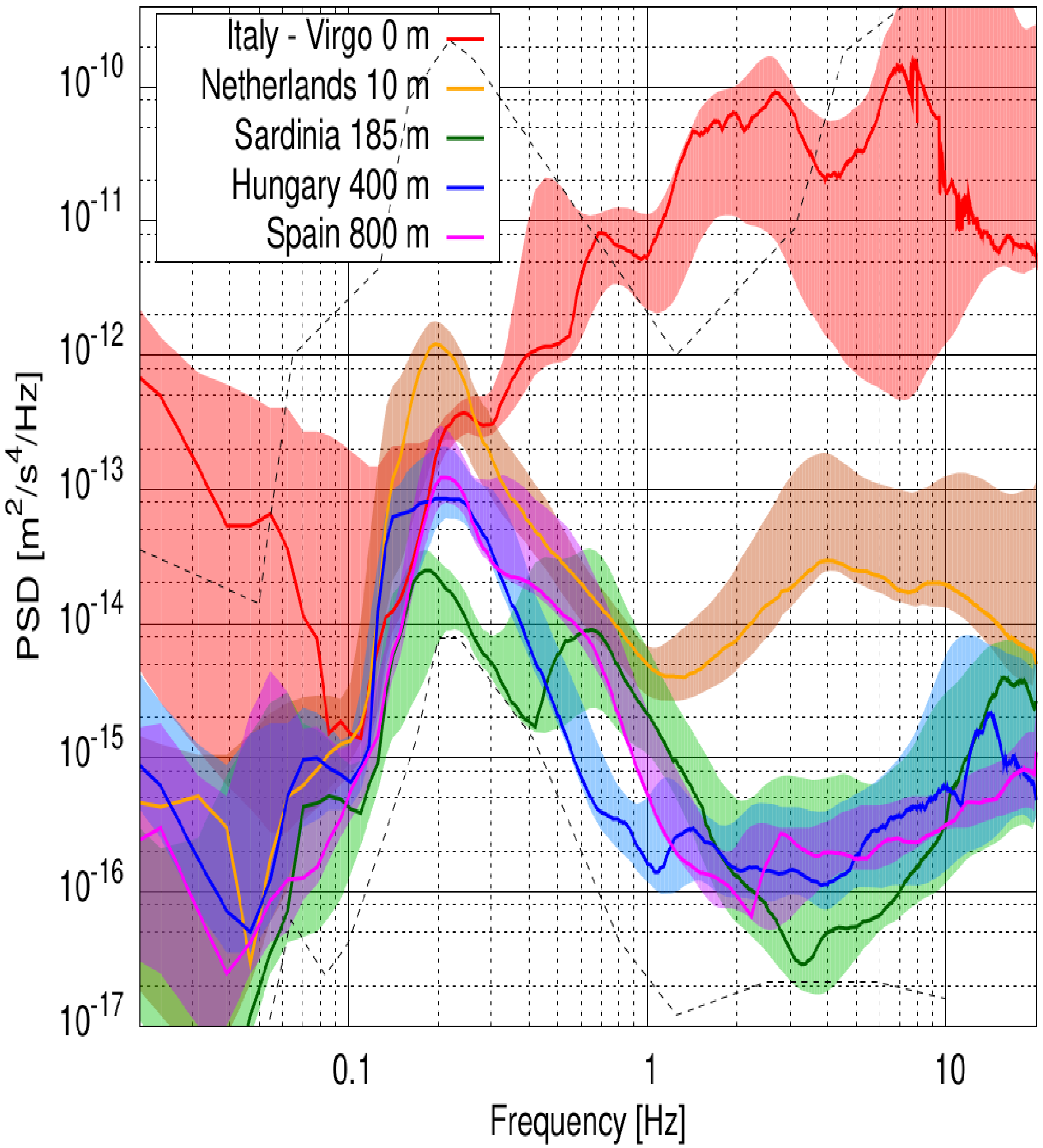

des: beam position

length coupling

or

V during O2

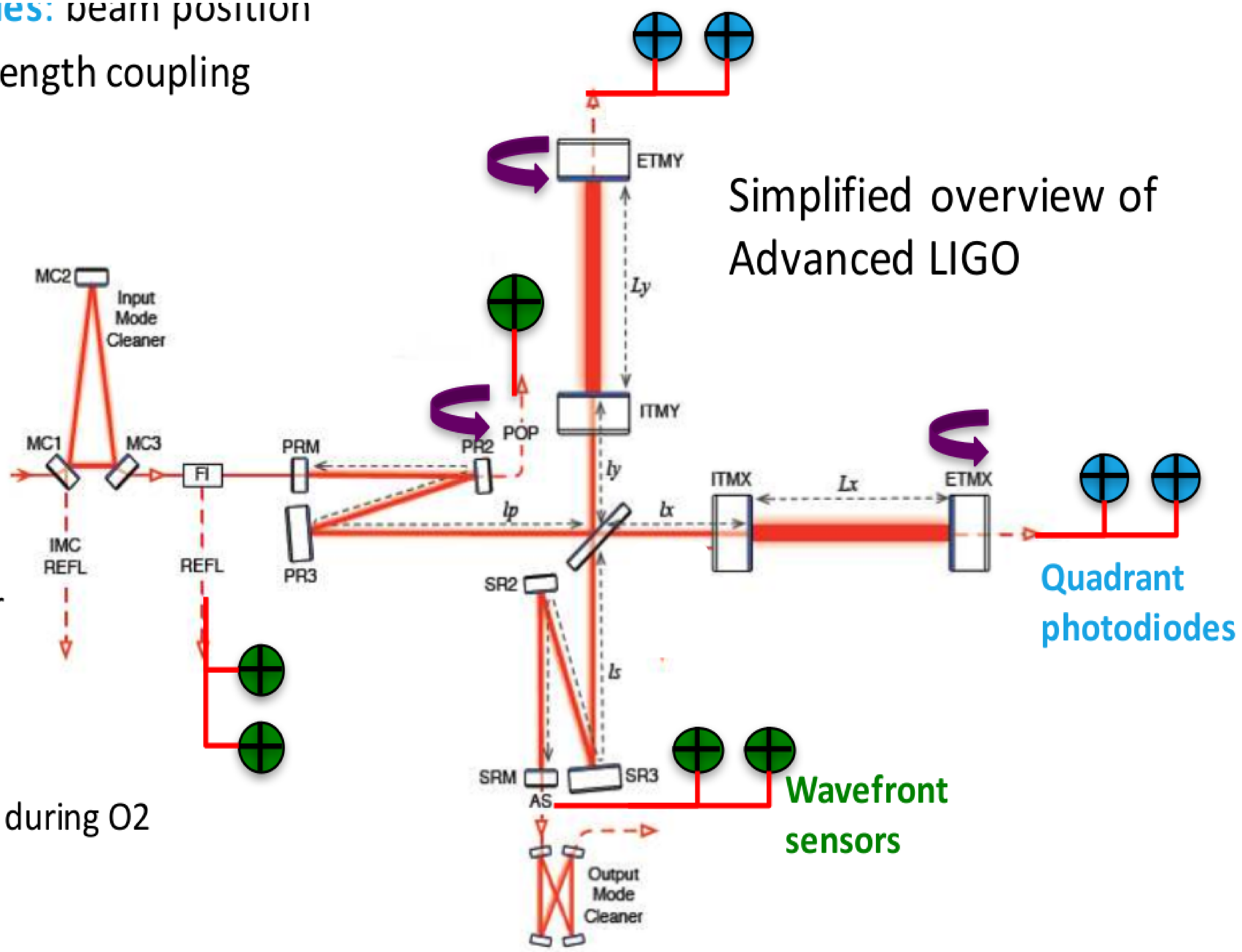

Simplified overview of Advanced LIGO

Quadrant photodiodes

Wavefront sensors

Alignment sensing and control

- WFS, QPD
- Sigg-Sidles

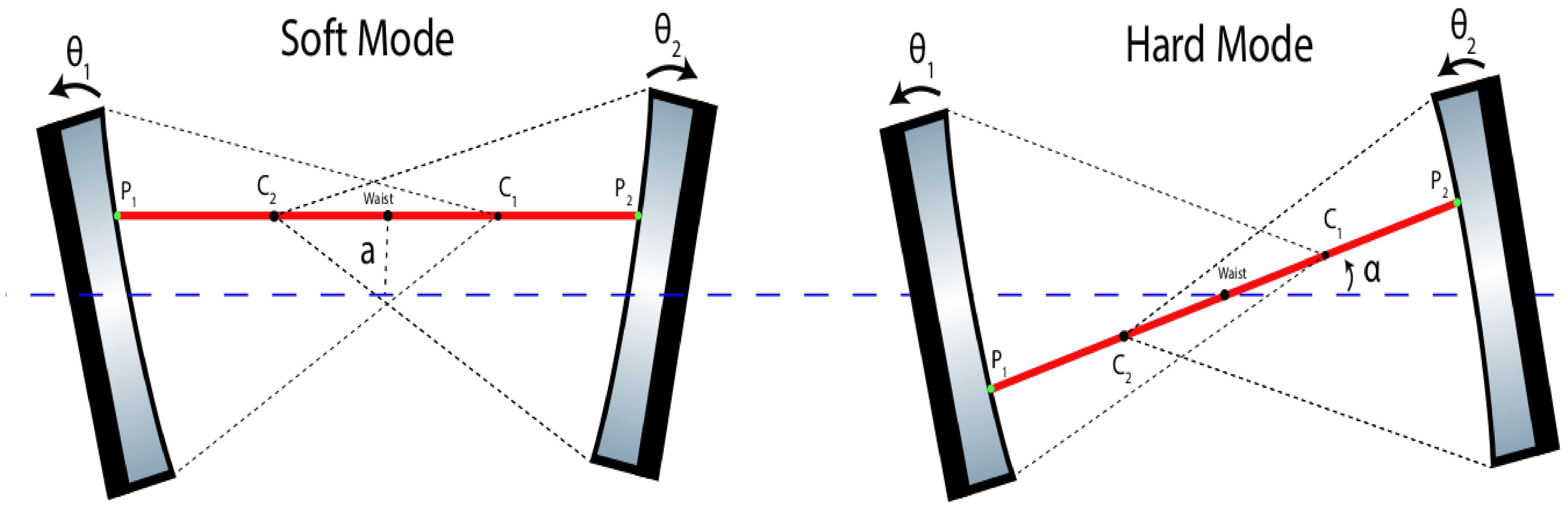

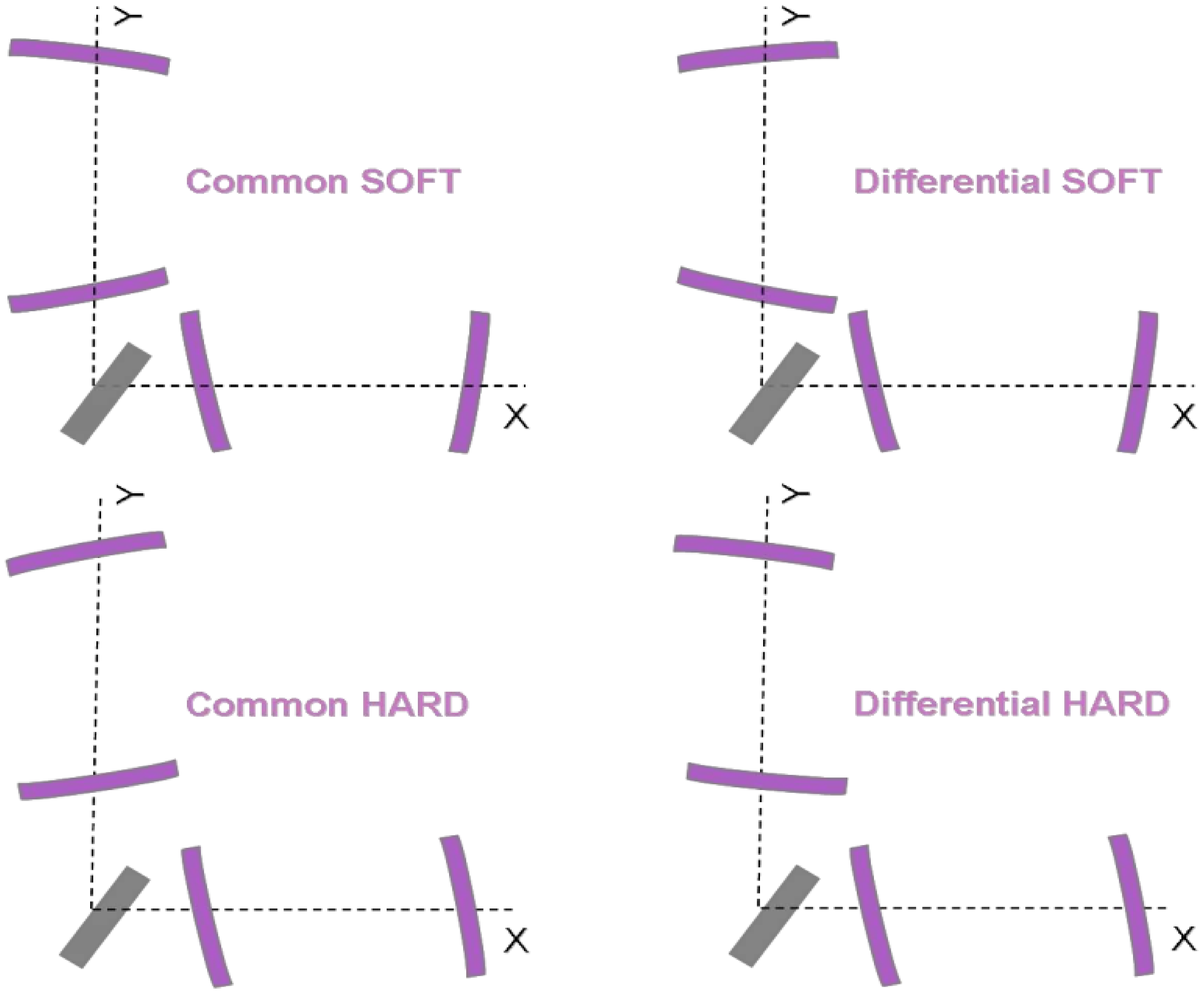

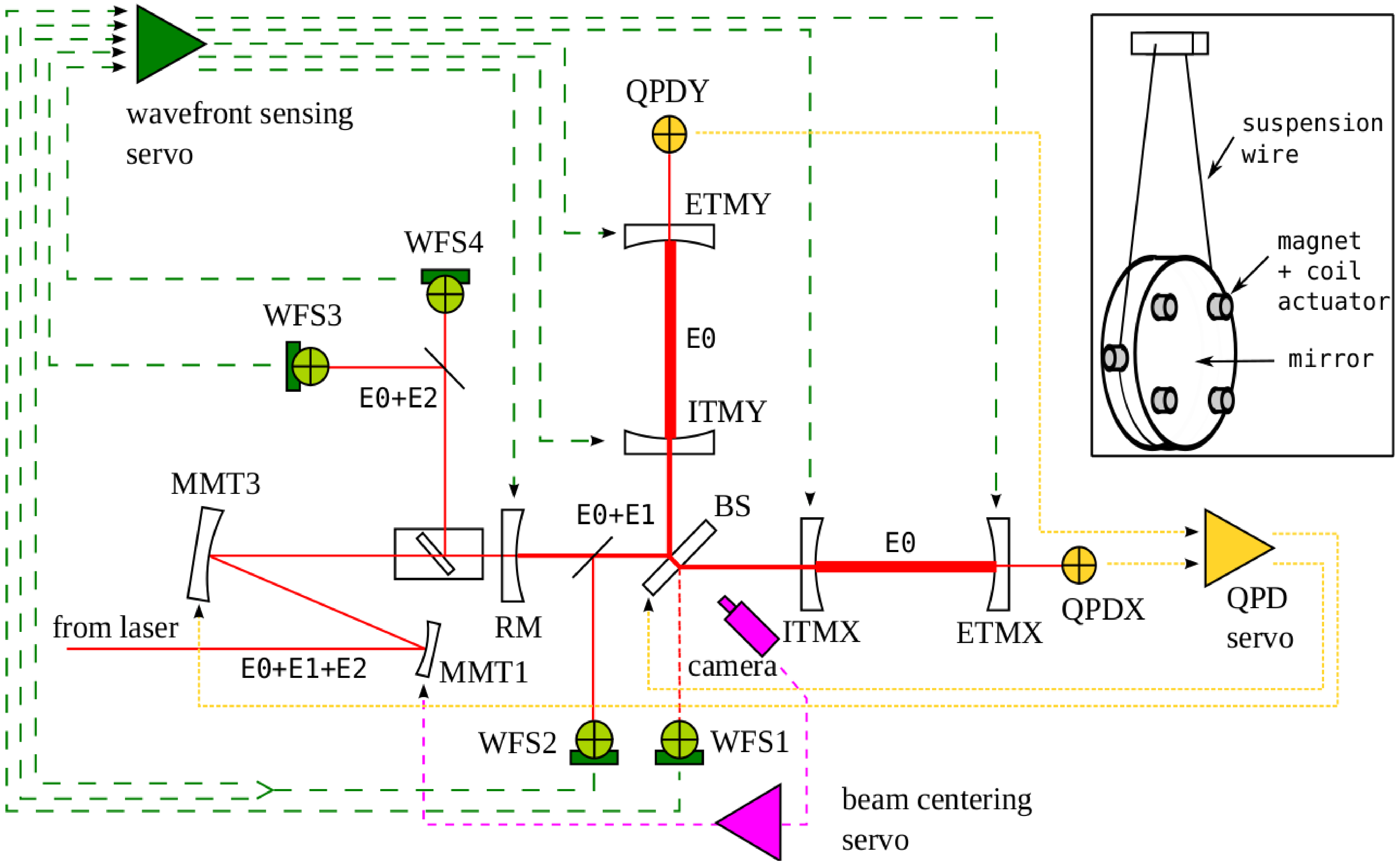

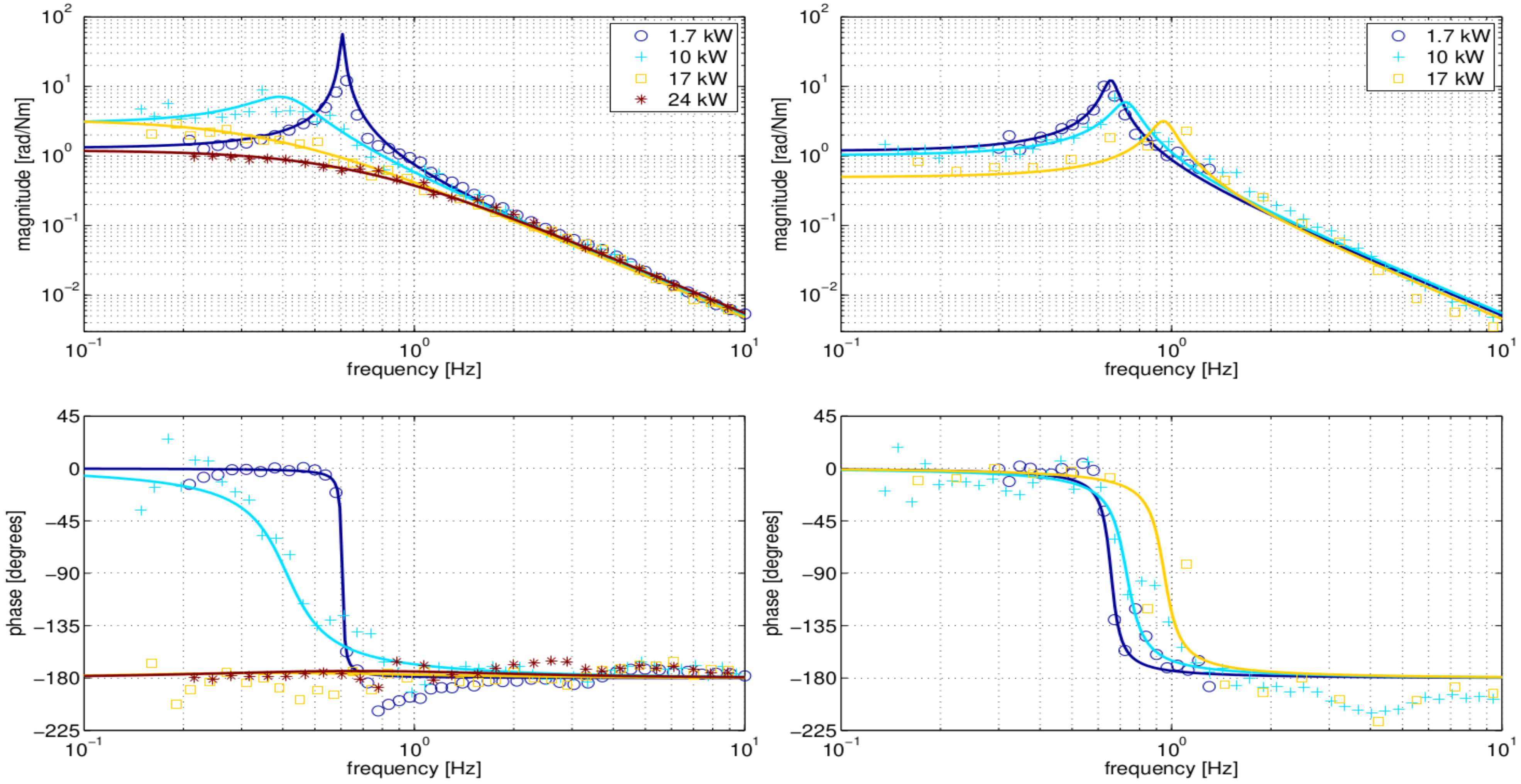
magnitude [rad/Nm]
frequency [Hz]
phase [degrees]
1.7 kW
10 kW
17 kW
24 kW
10^{2}
10^{1}
10^{0}
10^{-1}
10^{-2}
45
0
−45
−90
−135
−180
−225

(a)

(b)

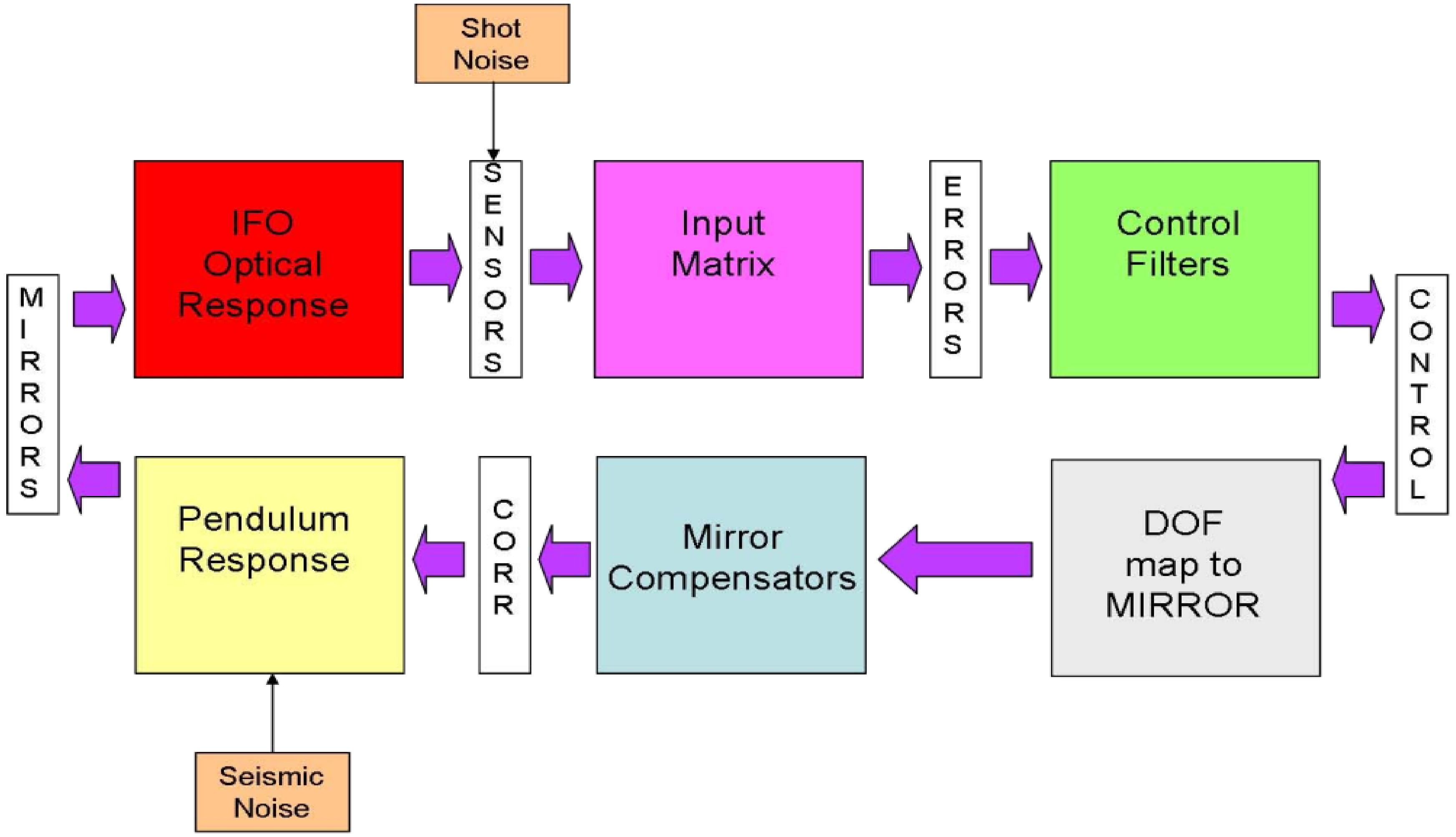
Shot Noise
MIRRORS
IFO Optical Response
SENSORS
Input Matrix
ERRORS
Control Filters
CONTROL
DOF map to MIRROR
Mirror Compensators
CORR
Pendulum Response
Seismic Noise

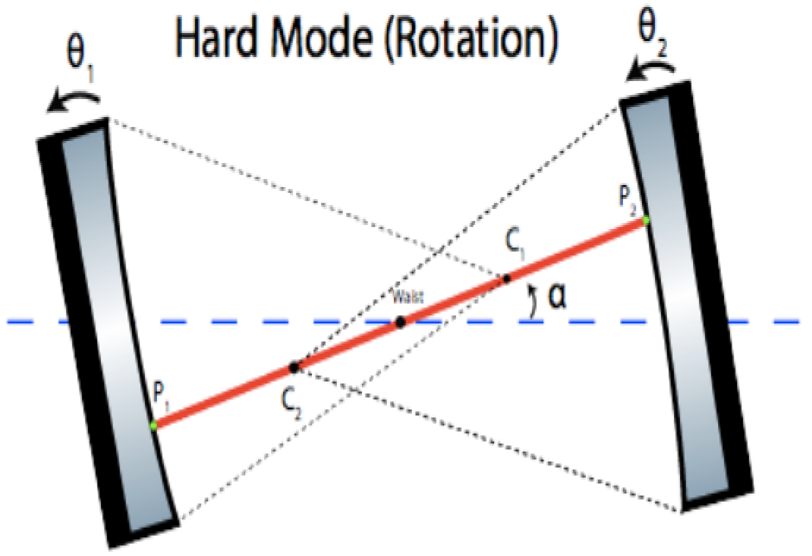
Hard Mode (Rotation)
θ_1
θ_2
P_1
P_2
C_1
C_2
Waist
α

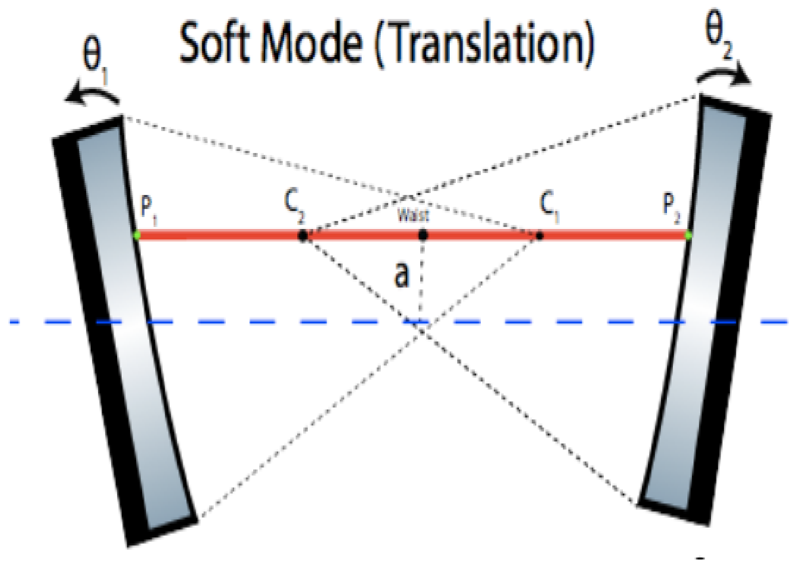
Soft Mode (Translation)
θ_1
θ_2
P_1
P_2
C_1
C_2
Waist
a

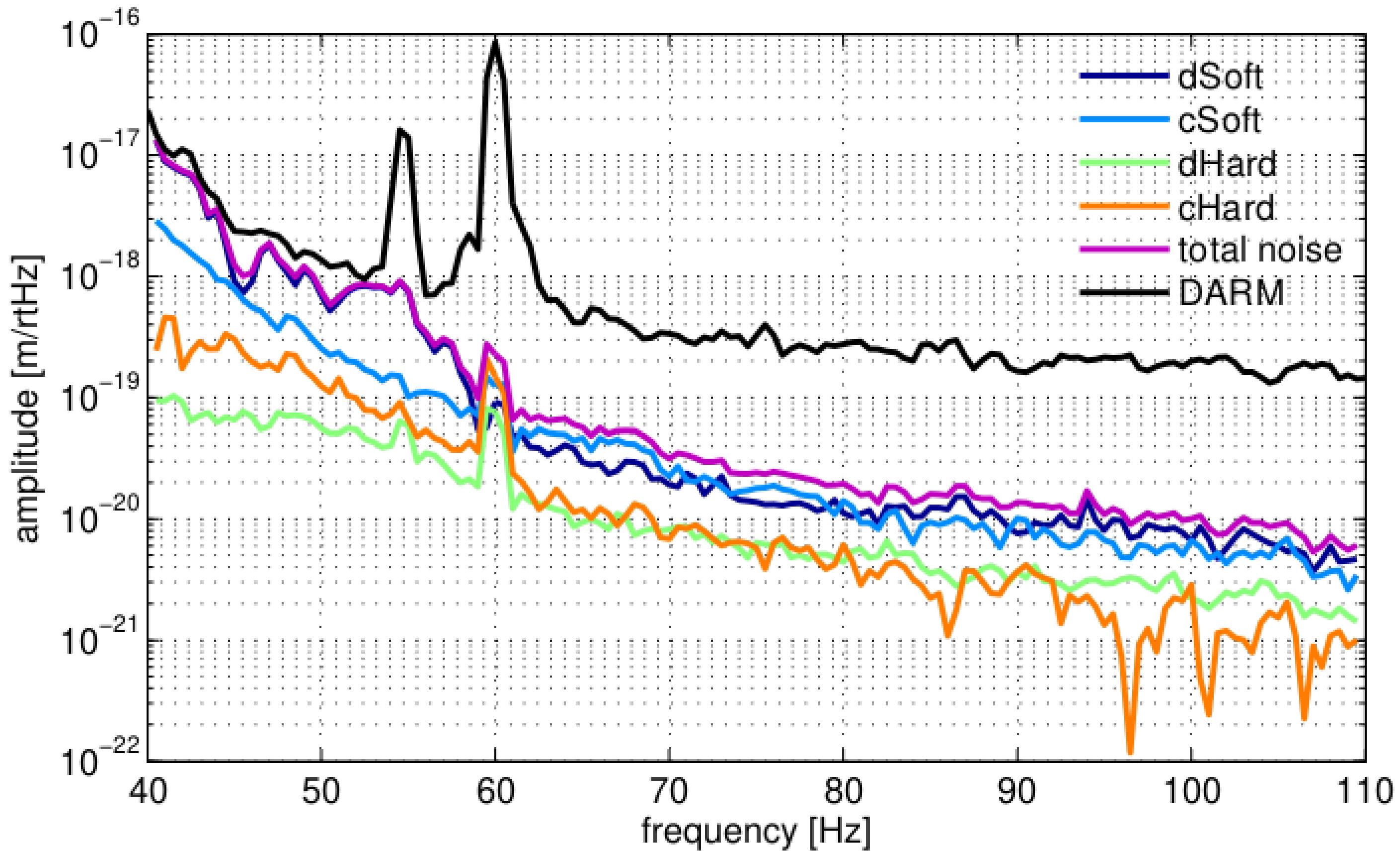
amplitude [m/rtHz]
frequency [Hz]
dSoft
cSoft
dHard
cHard
total noise
DARM
10^{-16}
10^{-17}
10^{-18}
10^{-19}
10^{-20}
10^{-21}
10^{-22}
40
50
60
70
80
90
100
110

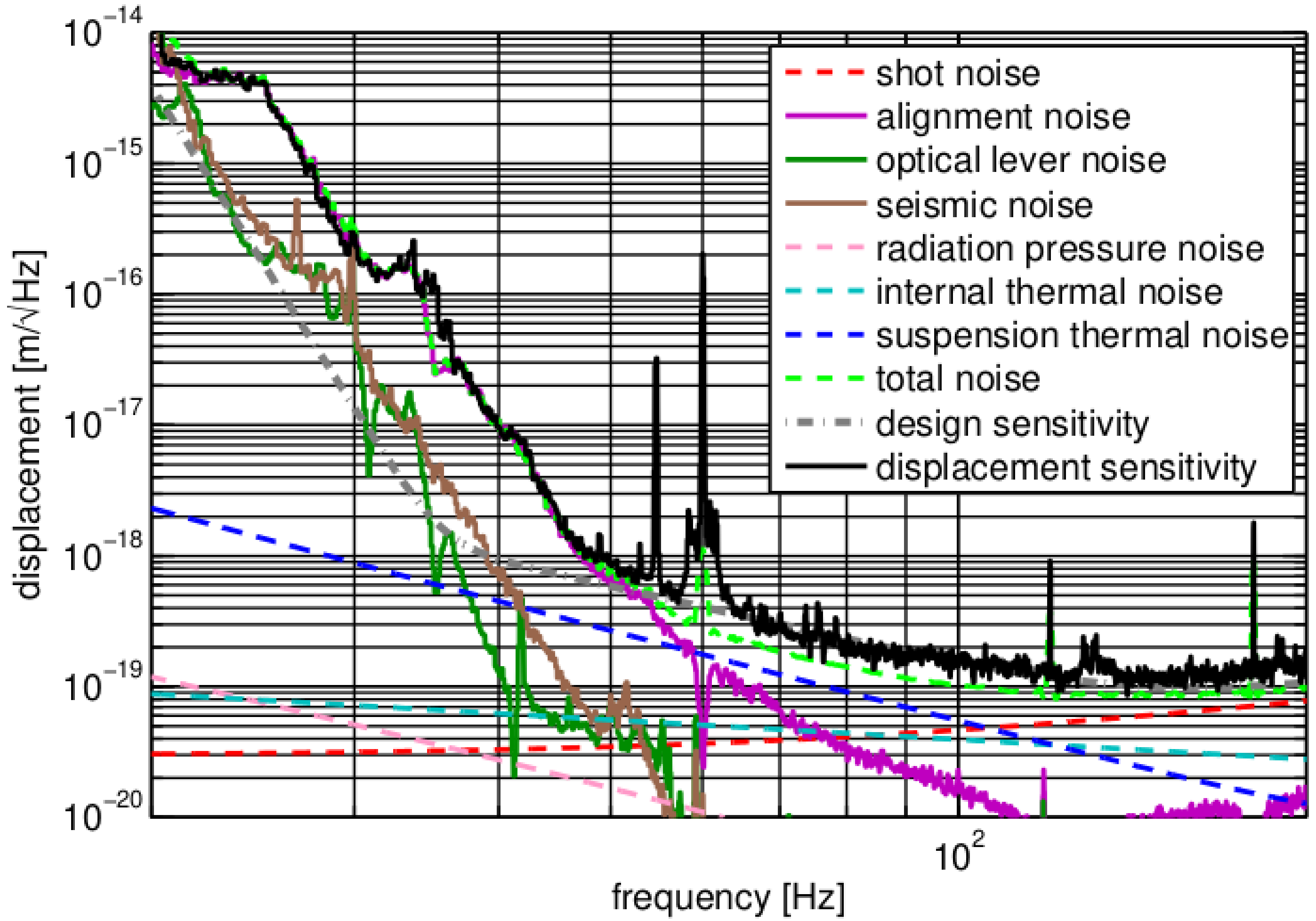

shot noise
alignment noise
optical lever noise
seismic noise
radiation pressure noise
internal thermal noise
suspension thermal noise
total noise
design sensitivity
displacement sensitivity
displacement [m/√Hz]
10^{-14}
10^{-15}
10^{-16}
10^{-17}
10^{-18}
10^{-19}
10^{-20}
10^{2}
frequency [Hz]

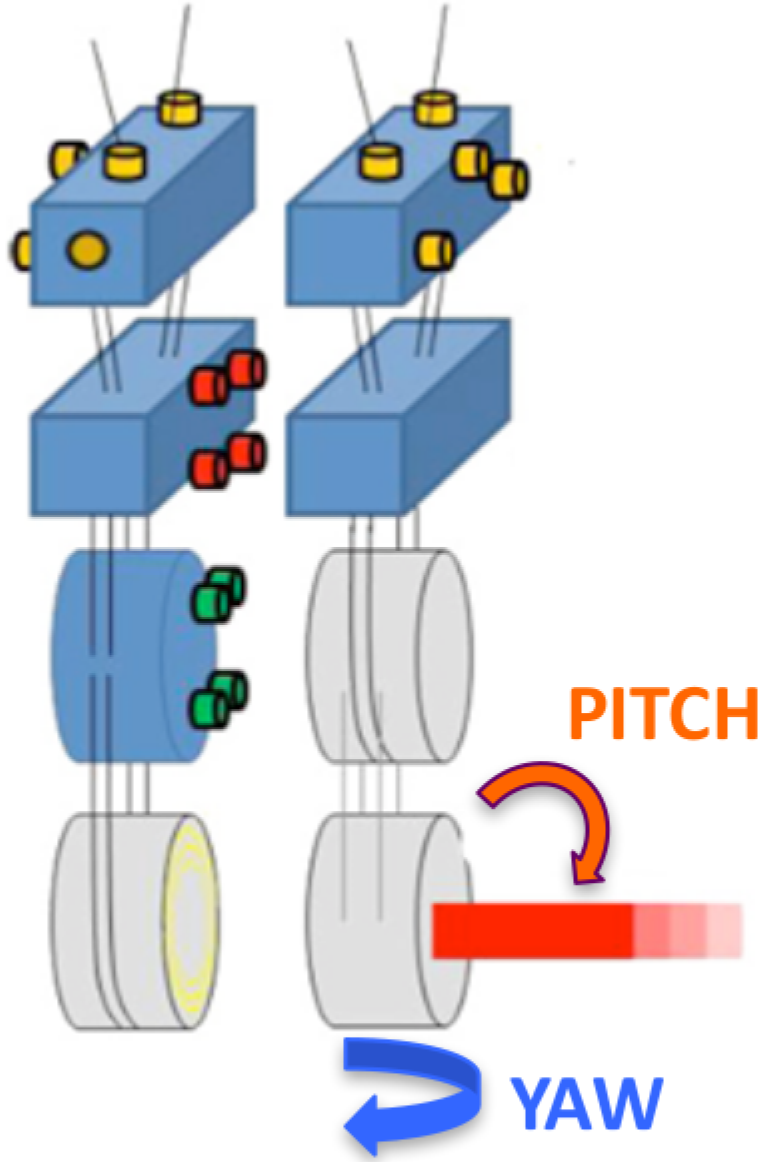

PITCH
YAW

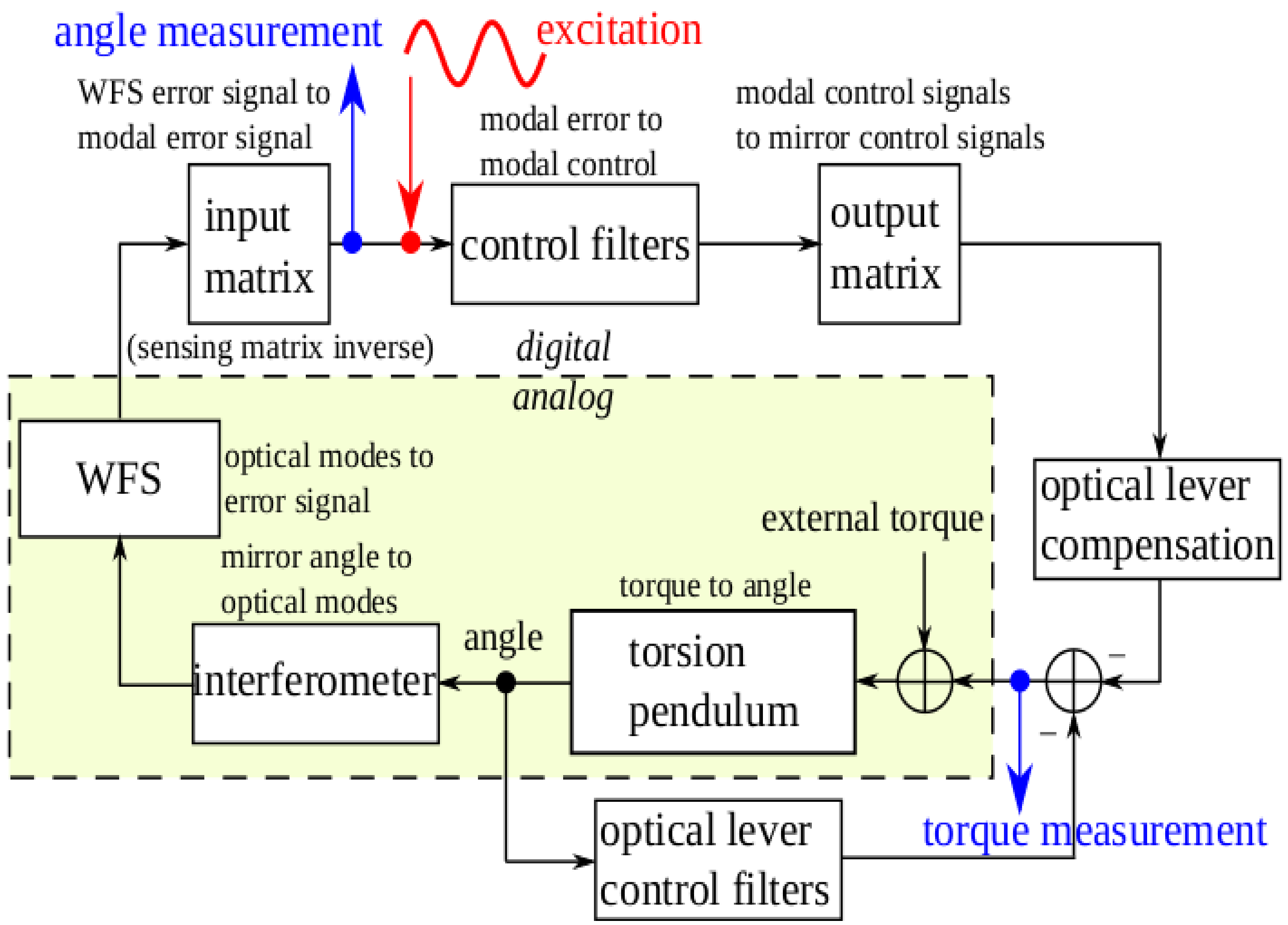

angle measurement
excitation
WFS error signal to modal error signal
modal error to modal control
modal control signals to mirror control signals
input matrix
control filters
output matrix
(sensing matrix inverse)
digital
analog
WFS
optical modes to error signal
mirror angle to optical modes
external torque
torque to angle
optical lever compensation
angle
interferometer
torsion pendulum
optical lever control filters
torque measurement
−
−

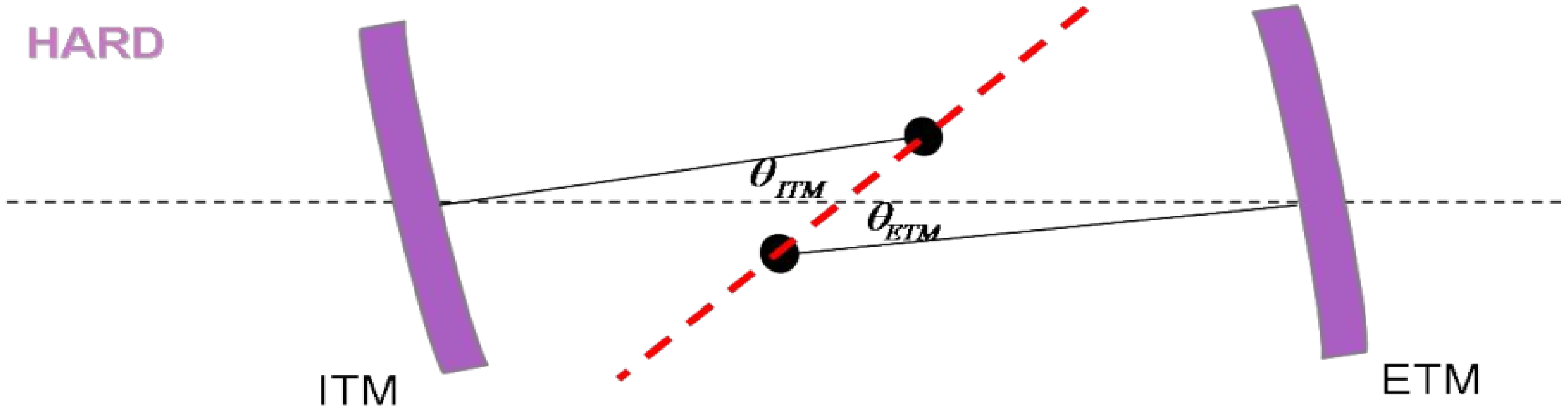

HARD
θ_{ITM}
θ_{ETM}
ITM
ETM

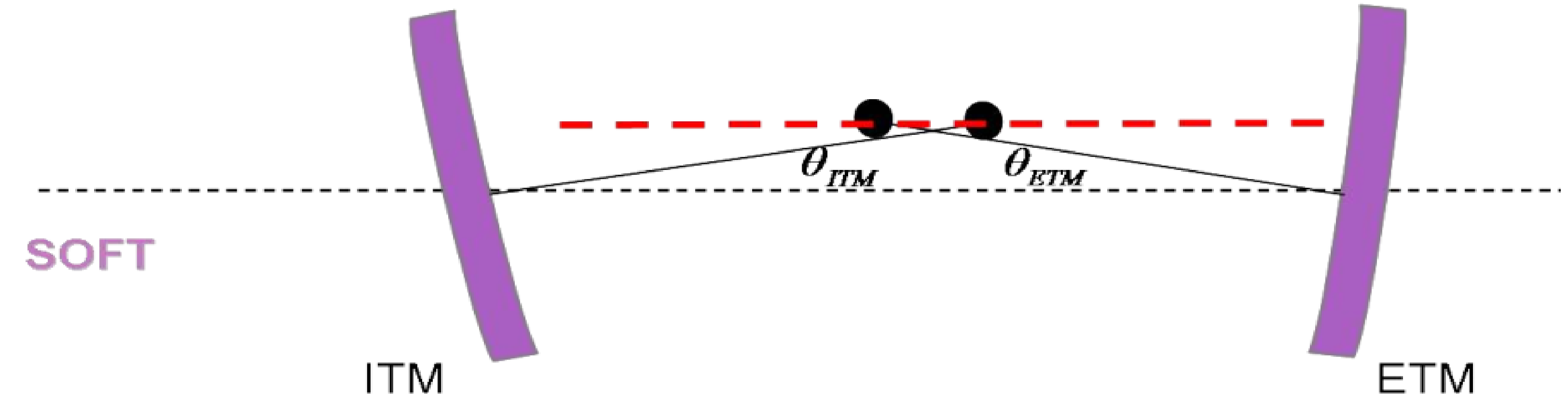

θ_{ITM}
θ_{ETM}
SOFT
ITM
ETM

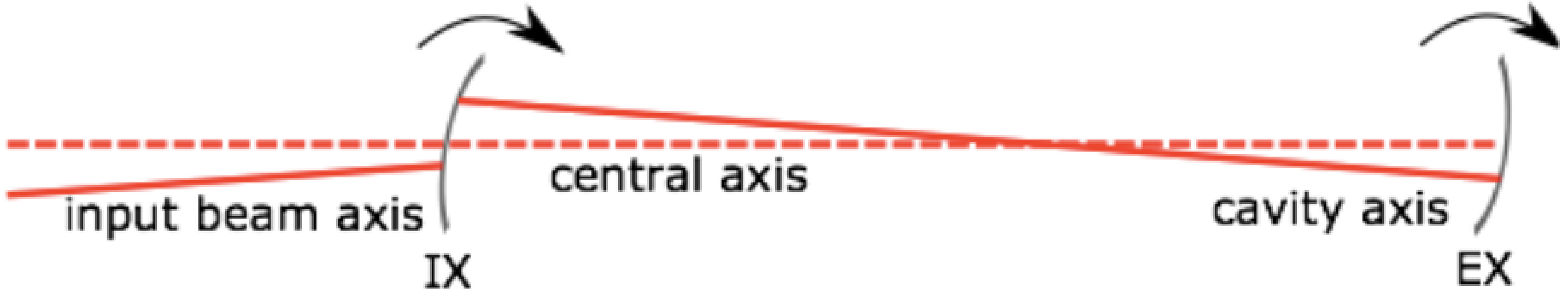

central axis
input beam axis
cavity axis
IX
EX

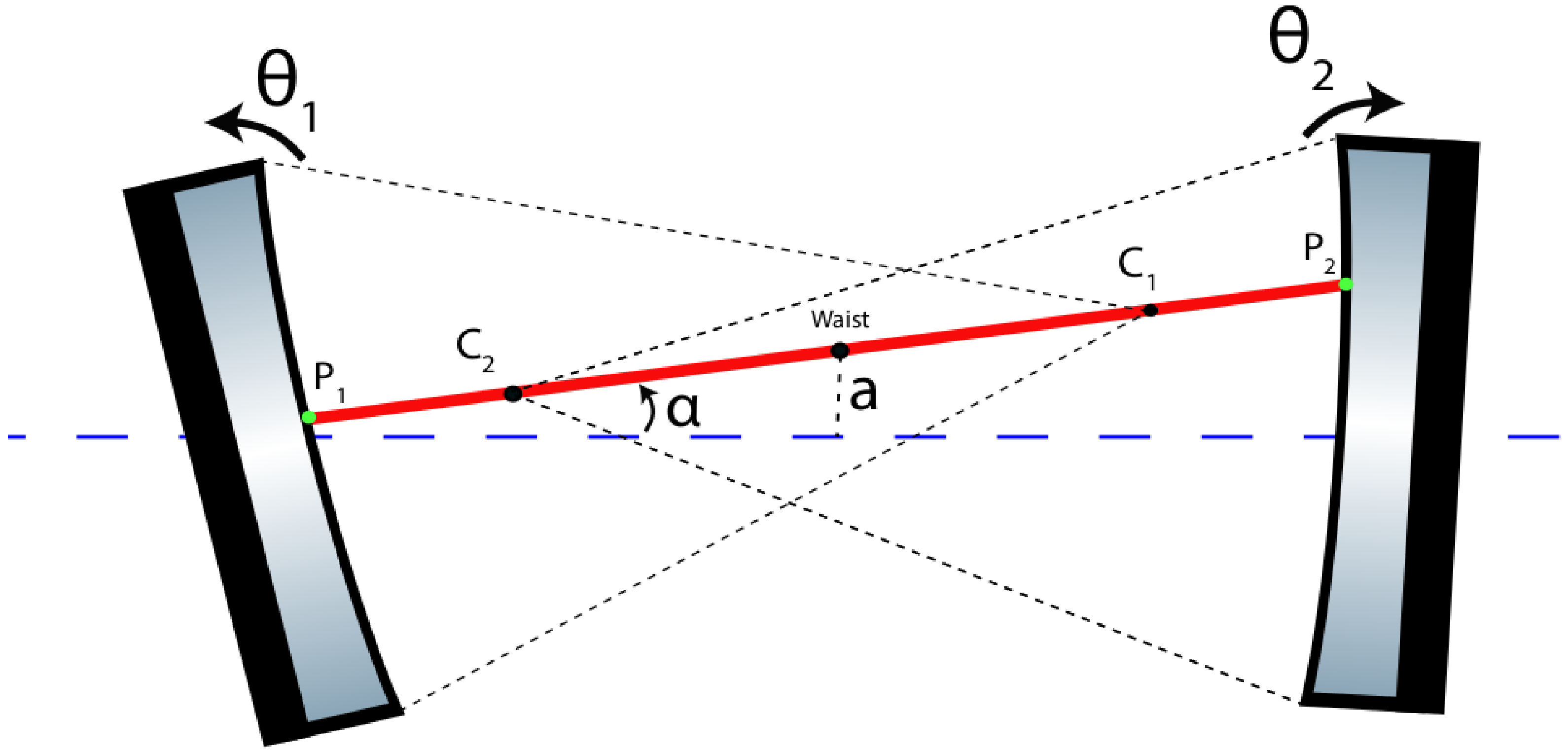

$$\hat{\Delta L}(f) = \hat{d}_{Spot}(f) * \hat{\theta}_{Mirror}(f)$$

ASC - allows us to operate IFO with angular mechanics dominated by RP

the proposed solution rotates the control basis to one that naturally represents the eigenmodes of the mirror motions coupled by RP to understand how the cavity dynamics are affected by RP it is useful to diagonalize the coupled eq's of the mirror motion into 2 normal cavity modes

Sidles-Sigg - the RP torque either softens or stiffens the mechanical springs

controller - linear filter, linear feedback, LP filter lot of gain at lf and and you surpress hf noise, tuned in nice way with UGF

you need 12 states to represent tf's between 2 points (internal states)

e.g., that the ML feedback control will be developed and tested with the time-domain simulation,

ASC ALLOWS US TO OPERATE IFO WITH ANGULAR MECHANICS DOMINATED BY RP; also to maximize the power coupled into the opical system, maintain the good quality of interference at the antisymmetric port, limit couplings to technical noise sources;; the alignement of optical axis of the IFO cavities as well as the centering of the BS on the optics;; TO KEEP IFO AT HIGH POWER, BEAM ALIGNEMENT CONDITION TO OPERATE

IFO STABLE AT HIGH POWER the proposed solution rotates the control basi to one that naturally represents the eignemodes of mirror motions coupled by RP

the most significant coupling of angular motion to cavity length occurs when the BS is off-center from the mirror's axis of rotation

the combination of mirror angular motion and BS motion on the TM's changes the length of the arms -> increase in the sensed long. motion

actuators - converts electric current signal into a mechanical output by employing the well-known Lorentz force eq

as P increases torsional stiffnes large enough to dominate the dynamics of the mirror suspension

we construct the stiffnes matrix for coupled translations and rotations of the 2 mirrors, and we show that this matrix has a simple and physically illuminating analytic form rotation of control basis to one that naturally represents the eigenmodes of mirror motions coupled with RPN

hard mode - rotation of cavity axis

soft mode - vertical displacement of the cavity axis

common hard - orientation is the same in both arms (motion where optics of one FP cavity rotate in the same direction as the other cavity)

differential - rotations in opposite directions

pitch - rotation about the mirror's horizontal axis

yaw - rotation about the vertical axis

RP - couples eq's of motion of 2 mirrors - as a beam impigning a mirror off-center creates a torque, an opto-mechanical angular
spring is created due to the geometric relationship of beam displacements and mirror angles to understand how the cavity dynamics are affected by RP it is useful to diagonalize the coupled eq's of the mirror motion
into normal cavity modes
KNOWN AS THE SIDLES-SIGG EFFECT - RP PRESSURE torque EITHER SOFFTENS OR STIFFENS THE MECHANICAL springs
THE dominant wAY IN WHICH angular motion creates a change in cavity length is the convolution of BS motion with angular mirror motion
ASC - upto 55 Hz - BILINEAR PROCESS

YOU GO TO NORMAL MODE BASIS WHICH DECOUPLES THE EFFECTS OF RP IN 2 INDEPENDANT modes
because of the longitudinal to pitch coupling inherent in the suspension we expect the pitch motion to be larger than yaw one
Seismic Newtonian-noise in comparison with the ET-D instrumental-noise model (according to the reference sensitivity ET-D) Seismic Newtonian-noise in comparison with the ET-D instrumental-noise mode
In addition to the main quadruple suspension chain that supports the test mass, there will also be a nearly identical reaction chain placed 5 mm behind it (see fig. 244 right side). This chain will allow control forces for global angular and longitudinal degrees of freedom to be applied from a quiet platform. These forces will be hierarchically used, with large forces applied with coils and magnets between both the upper intermediate and penultimate masses but with fine control forces applied with an electrostatic drive (ESD). The ESD is a gold pattern deposited on the face of the final reaction mass and applies forces to the test mass with an electrostatic field. Local damping of all the low frequency suspension modes will be done with co-located sensors and actuators on the top mass to insure that any sensing noise will be well isolated from the test mass.

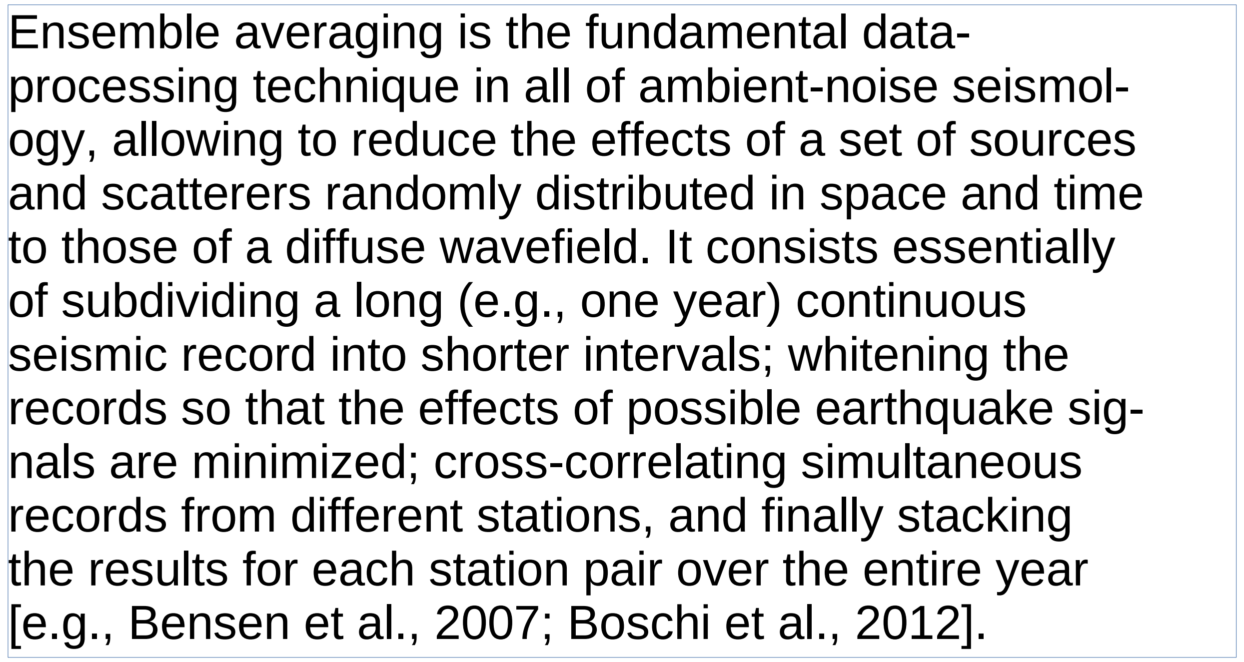

Ensemble averaging is the fundamental data-processing technique in all of ambient-noise seismology, allowing to reduce the effects of a set of sources and scatterers randomly distributed in space and time to those of a diffuse wavefield. It consists essentially of subdividing a long (e.g., one year) continuous seismic record into shorter intervals; whitening the records so that the effects of possible earthquake signals are minimized; cross-correlating simultaneous records from different stations, and finally stacking the results for each station pair over the entire year [e.g., Bensen et al., 2007; Boschi et al., 2012].

$$c_{ij}(f) = J_0(2\pi f|\vec{r}_j - \vec{r}_i|/c)$$

Pitch2DARM =
0.001*2./4000
psd_h = psd *
pitch2DARM ** 2

The Laser Interferometer Gravitational Wave Observatory (LIGO) operates a 40m prototype interferometer on the Caltech campus.
The primary mission of the prototype is to serve as an experimental testbed for upgrades to the LIGO interferometers and for
gaining experience with advanced interferometric techniques

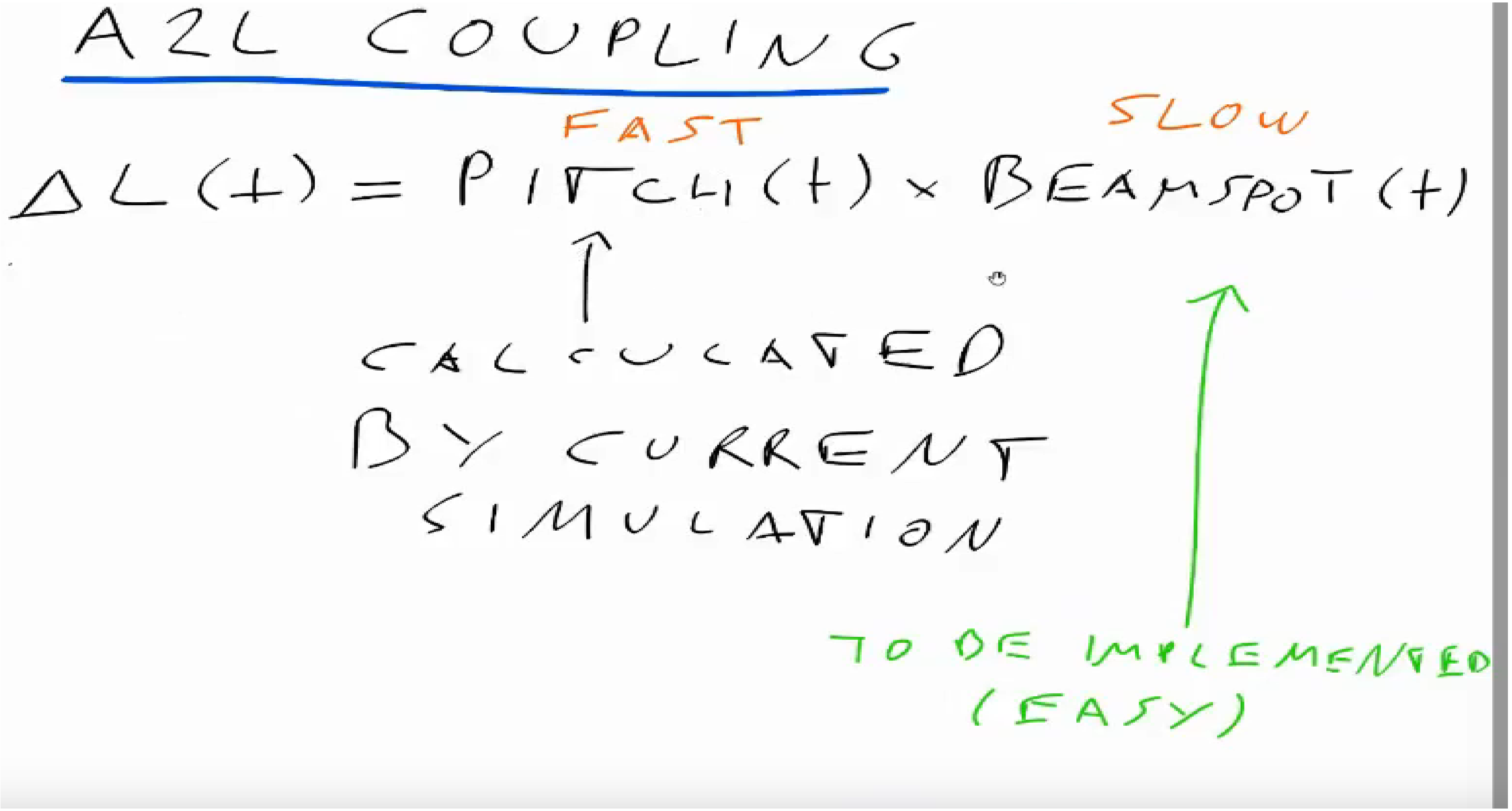

A2L COUPLING

$$\Delta L(t) = \overset{\text{FAST}}{\text{PITCH}(t)} \times \overset{\text{SLOW}}{\text{BEAMSPOT}(t)}$$

↑ CALCULATED BY CURRENT SIMULATION

↑ TO BE IMPLEMENTED (EASY)